Rate constant for the reaction $CH_3 + CH_3 \rightarrow C_2H_6$ at T = 155 K and model calculation of the CH_3 abundance in the atmospheres of Saturn and Neptune

Regina J. Cody,[1] Paul N. Romani,[1] Fred L. Nesbitt,[2] Mark A. Iannone,[3] Dwight C. Tardy,[4] and Louis J. Stief[1]

Received 20 December 2002; revised 29 July 2003; accepted 5 August 2003; published 15 November 2003.

[1] The column abundances of CH_3 observed by the Infrared Space Observatory (ISO) satellite on Saturn and Neptune were lower than predicted by atmospheric photochemical models, especially for Saturn. It has been suggested that the models underestimated the loss of CH_3 due to poor knowledge of the rate constant k of the CH_3 + CH_3 self-reaction at the low temperatures and pressures of these atmospheres. Motivated by this suggestion, we undertook a combined experimental and photochemical modeling study of the CH_3 + CH_3 reaction and its role in determining planetary CH_3 abundances. In a discharge flow-mass spectrometer system, k was measured at T = 155 K and three pressures of He. The results in units of cm^3 $molecule^{-1}$ s^{-1} are k(0.6 Torr) = 6.82×10^{-11}, k(1.0 Torr) = 6.98×10^{-11}, and k(1.5 Torr) = 6.91×10^{-11}. Analytical expressions for k were derived that (1) are consistent with the present laboratory data at T = 155 K, our previous data at T = 202 K and 298 K, and those of other studies in He at T = 296–298 K and (2) have some theoretical basis to provide justification for extrapolation. The derived analytical expressions were then used in atmospheric photochemical models for both Saturn and Neptune. These model results reduced the disparity with observations of Saturn, but not with observations of Neptune. However, the disparity for Neptune is much smaller. The solution to the remaining excess CH_3 prediction in the models relative to the ISO observations lies, to a large extent, elsewhere in the CH_3 photochemistry or transport, not in the CH_3 + CH_3 rate. *INDEX TERMS:* 0317 Atmospheric Composition and Structure: Chemical kinetic and photochemical properties; 0343 Atmospheric Composition and Structure: Planetary atmospheres (5405, 5407, 5409, 5704, 5705, 5707); *KEYWORDS:* methyl radical combination, low temperature rate constant, Lindemann expression, Saturn, Neptune, atmospheric photochemical models

Citation: Cody, R. J., P. N. Romani, F. L. Nesbitt, M. A. Iannone, D. C. Tardy, and L. J. Stief, Rate constant for the reaction CH_3 + $CH_3 \rightarrow C_2H_6$ at T = 155 K and model calculation of the CH_3 abundance in the atmospheres of Saturn and Neptune, *J. Geophys. Res.*, *108*(E11), 5119, doi:10.1029/2002JE002037, 2003.

1. Introduction

[2] The recent detection of the methyl free radical in the atmospheres of Saturn [*Bézard et al.*, 1998] and Neptune [*Bézard et al.*, 1999] provide the impetus for the present study. These are the first observations of a hydrocarbon free radical in the atmospheres of the outer planets. The levels of CH_3 observed on Saturn and Neptune were lower than predicted by atmospheric models, especially for Saturn. It has been suggested [*Bézard et al.*, 1998, 1999; *Atreya et al.*, 1999; *Moses et al.*, 2000; *Lee et al.*, 2000] that the previous models greatly underestimate the loss of CH_3 due to poor knowledge of the rate of the self-reaction

$$CH_3 + CH_3 + M \rightarrow C_2H_6 + M \qquad (1)$$

at the low temperatures and pressures of these atmospheric systems. For the atmospheric models, appropriate conditions would be T = 140–200 K, P < 0.2 Torr and M = H_2/He. C_2H_6 is observed in the atmospheres of the outer planets and reaction (1) is the dominant source of this molecule.

[3] With few exceptions, most of the more than 60 published laboratory studies have been performed at higher temperatures (T $\geq$ 296 K) or higher pressures (P $\geq$ 5 Torr) or with inappropriate bath gases M (usually Ar). Aside from our recent study [*Cody et al.*, 2002] of k_1 at T = 298 and 202 K and P = 0.6, 1.0 and 2.0 Torr He, the only studies of this reaction at T < 296 K, P < 5 Torr He are as follows. The two reports available of studies below room temperature are at

[1]Laboratory for Extraterrestrial Physics, NASA Goddard Space Flight Center, Greenbelt, Maryland, USA.
[2]Department of Chemistry, Catholic University of America, Washington, DC, USA.
[3]Department of Chemistry, Millersville University, Millersville, Pennsylvania, USA.
[4]Department of Chemistry, University of Iowa, Iowa City, Iowa, USA.

0148-0227/03/2003JE002037

T = 200 K [*Walter et al.*, 1990] and T = 250, 273 K [*Parkes et al.*, 1976] but both are at high pressures. We are aware of only a few published studies at pressures below 5 Torr or employing He as a bath gas [*Slagle et al.*, 1988; *Walter et al.*, 1990; *Deters et al.*, 1998a, 1998b; *Stoliarov et al.*, 2000]. The paucity of data at low temperatures and low pressures reflects both experimental convenience and the importance of the $CH_3 + CH_3$ reaction in hydrocarbon combustion chemistry.

[4] *Cody et al.* [2002] previously reported measurements of k_1 at T = 298 and 202 K using the discharge flow-mass spectrometric technique (DF-MS). In that study, Cody et al. briefly summarize the numerous experimental and theoretical studies of this reaction. The experimental results at T = 298 K and P = 0.6 and 1.0 Torr He were compared with the few previous low-pressure studies with M = He. They also measured k_1 at T = 202 K and P = 0.6, 1.0 and 2.0 Torr He (the limits of the system) which provided the first measurements of this rate constant in the fall-off region at T < 296 K. This allowed for verification of the recent calculations by *Klippenstein and Harding* [1999] on the pressure dependence of k_1 at T = 200 K when modified from M = Ar to M = He.

[5] We report here on measurements of k_1 at T = 155 K again using the DF-MS technique. This temperature is representative of that in the regions of the atmospheres of Saturn and Neptune where methyl radical formation and reaction are occurring. This study provides the first measurement of the rate constant for methyl recombination at a temperature below 200 K. Using both experimental and theoretical data, analytical expressions are derived for k_1 as a function of pressure and temperature. These expressions, along with other relevant information, are used in an atmospheric photochemical model to provide predicted levels of CH_3 in the atmospheres of Saturn and Neptune for comparison with observations [*Bézard et al.*, 1998, 1999].

2. Experimental Section

[6] The apparatus used in our experiments consists of a discharge flow system coupled via a collision-free sampling system to a quadrupole mass spectrometer. Figure 1 shows a schematic diagram of the system. A separate gas handling line was used to purify reagents and prepare and store gas mixtures for delivery to the flow tube. Since the original description of the apparatus was published [*Brunning and Stief*, 1986], several major changes have been made and are incorporated into the following revised description.

2.1. Discharge Flow System

[7] The experiments were performed in a newly fabricated Pyrex flow tube about 60 cm in length and 2.5 cm in diameter. The inner surface of the flow tube is lined with Teflon FEP, which yields an inner diameter of 2.01 cm for the flow region. The flow tube is fitted with a movable Pyrex injector (6 mm outer diameter) whose position can be varied between the distances d = 3 and 44 cm from the sampling pinhole leading to the mass spectrometer. Gas flows enter the flow tube through the movable injector and sidearms upstream of the reaction zone, one of which is encircled by a microwave discharge (2450 MHz) cavity for the generation of atomic or free radical species. These gases were pumped at constant linear velocity (v = 2200–2600 cm/s) along the tube and through a short 1–2 cm region between the end of the flow tube and the first pinhole; the flow is perturbed in this region. In the calculation of the linear flow velocity, the plug flow assumption is made. The flow velocity is calculated from the gas constant, temperature, cross-sectional area of the flow tube, total gas flow and total pressure.

[8] The flow tube pressure was monitored when the injector was at the center of the reaction zone (d = 20 cm) using a capacitance manometer (MKS Baratron, 10 Torr head). To determine the pressure gradient along the flow tube, we temporarily coupled the capacitance manometer to the movable injector. The pressure gradient along the flow tube between d = 3 and 44 cm was less than ±5% of the measured value at the center of the reaction zone. Helium carrier gas flows and reagent flows (CH_4, F_2/He, Cl_2/He) were measured and controlled by separate mass flow controllers (MKS). Small corrections to the indicated flow rates for the dilute F_2 and Cl_2 in He flows were made to allow for the contribution of F_2 and Cl_2 to the heat capacity of the dilute mixtures.

[9] An annular Pyrex jacket surrounds the entire flow tube from the outlet end near the sampling pinhole to 60 cm upstream. The flow tube is cooled by circulating nitrogen gas through the jacket. The nitrogen gas is supplied by a nitrogen liquid-to-gas converter Dewar and the gas is cooled by passage through a copper coil immersed in liquid nitrogen (T = 77 K). The temperature of the flow tube is controlled by varying the flow of the gaseous nitrogen with a valve located before the copper coil. The temperature of the gas inside the flow tube is measured in the middle of the reaction zone by a sheathed iron-constantan (Type J) thermocouple (Omega, 1/8 inch). The temperature profile along the length of the flow tube was measured by movable injectors containing either Type K or J thermocouples. The temperature is constant to within ±6 K from a distance d = 4 cm from the sampling pinhole to d = 44 cm. From d = 4 cm to the sampling pinhole there is a gradual temperature gradient. The flow tube and jacket are insulated with several layers of fiberglass sheeting with a final layer of 10-mm thick foam rubber. Lines leading from the cooling coil are also insulated.

2.2. Sampling System and Mass Spectrometer

[10] The flow tube is coupled via a glass-metal O-ring joint to the two-stage stainless-steel collision free sampling system [*Brunning and Stief*, 1986], which was designed and assembled on the basis of those constructed by Clyne and coworkers [*Clyne and Watson*, 1974; *Clyne and MacRobert*, 1980]. Efficient collision-free sampling of the flow tube gases is achieved by using two collinear pinholes spaced two cm apart. Both pinholes were drilled in demountable stainless-steel disks, the first having a diameter of 1.5 mm and the second a diameter of 1.75 mm.

[11] The two differential pumping stages were constructed of stainless steel, and all flanges are sealed by copper gaskets. Each stage is pumped by a 6-in. diffusion pump. Both pumps are filled with polyphenyl ether pump fluid (Santovac) which has a low backstreaming rate, a low vapor pressure (4×10^{-10} Torr) at T = 298 K, and is resistant to oxidation and thermal decomposition. A Freon-cooled chevron baffle (CVC) was incorporated into the first stage, and an automatically filled liquid nitrogen trap was

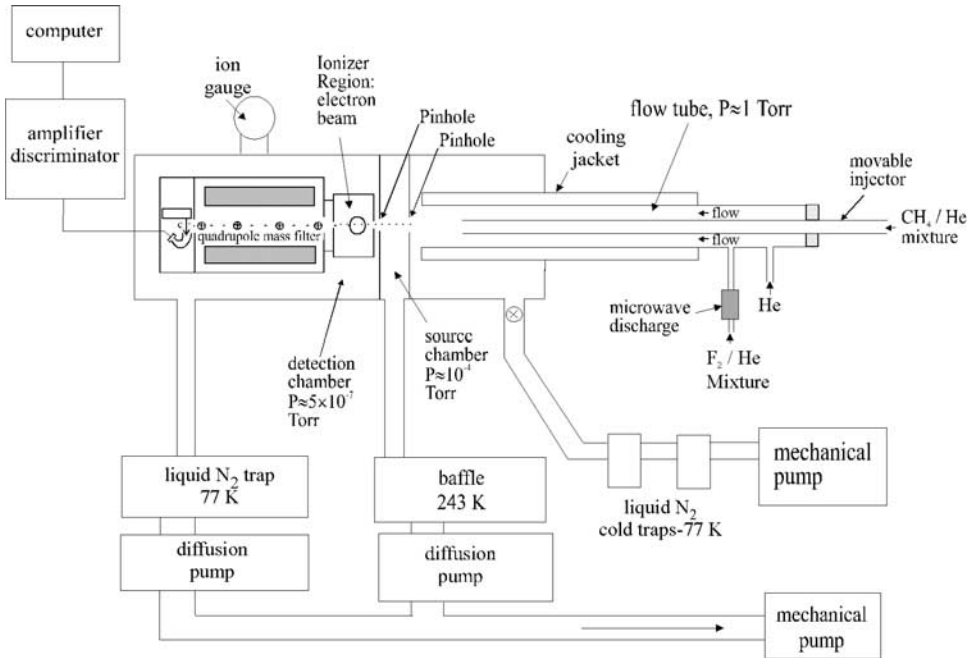

Figure 1. Diagram of the discharge flow-mass spectrometer system.

added to the second stage to minimize contamination of the mass spectrometer and walls of the chamber resulting from back diffusion. A molecular-sieve foreline trap is used to trap mechanical-pump oil.

[12] A quadrupole mass spectrometer (ABB Extrel Merlin) is used in conjunction with an off-axis channeltron multiplier (Burle Electro-Optics). Signals are passed through an amplifier-discriminator (Advanced Research Instruments Corporation) and into the Merlin computerized control unit where ion counting is performed. The Merlin computer also controls the operation of the mass spectrometer. The quadrupole head is housed within a liquid nitrogen cooled copper shroud that reduces the background pressure and background signal, thereby increasing the detection limit of the mass spectrometer. The residual background pressure in the mass spectrometer was typically 2×10^{-8} Torr. At a flow tube pressure of 1 Torr the pressure in the mass spectrometer chamber rises to about 5×10^{-7} Torr.

2.3. Production and Monitoring of CH_3

[13] Fluorine atoms were produced at the upstream end of the flow reactor by passing molecular F_2 diluted in He through a microwave discharge (50 W, 2450 MHz). The discharge region consists of a 3/8 in. inner diameter ceramic tube coupled via Teflon Swagelok connectors to a glass discharge arm. For $[F_2] \geq 4 \times 10^{12}$ molecule cm^{-3}, about 50–90% of the F_2 was dissociated in the discharge. The CH_4 reactant was admitted via the Pyrex movable injector. At the tip of the movable injector CH_3 was produced via the fast reaction

$$F + CH_4 \rightarrow CH_3 + HF \qquad (2)$$

where k_2 (155 K) = 3.0×10^{-11} cm^3 $molecule^{-1}$ s^{-1} [*DeMore et al.*, 1997]. Methane was in large excess ($[CH_4]/[F] \cong 100–200$) with concentrations of about 1.0×10^{15} molecule cm^{-3}. These conditions ensured rapid and quantitative conversion of F to CH_3. The large excess of CH_4 prevented secondary loss of CH_3 via reaction with F. In addition, the subsequent reaction of CH_3 with residual F_2 to form $CH_3F + F$ is followed by very rapid regeneration of CH_3 via reaction (2). The large concentrations of CH_4 required to achieve these desirable features were only possible in the present experiments due to the complete absence of dissociative ionization of CH_4 to yield CH_3^+. A disadvantage of this method of generation of CH_3 is that the more appropriate bath gas H_2 cannot be employed instead of He since F reacts rapidly with H_2.

[14] Methyl radicals were detected at m/z = 15 following low-energy electron ionization. The use of low electron energies (11 eV) avoided formation of CH_3^+ from dissociative ionization of the CH_4 reactant present in great excess and from the equilibrated C_2H_6 product. Mass scans were recorded for the region 14.5–15.5 amu and signals were taken as the integrated area of the m/z = 15 peak. Signals were typically averaged for 30–60 s for each injector position and several scans were recorded for each position. The observed signal was corrected for a small ($\leq$1%) background signal measured with the microwave discharge off.

2.4. Determination of $[F]_0$

[15] The absolute concentration of fluorine atoms used to generate CH_3 was determined by measuring the consumption of Cl_2 in the fast titration reaction:

$$F + Cl_2 \rightarrow Cl + FCl \qquad (3)$$

where $k_3 = 6.0 \times 10^{-11}$ cm^3 $molecule^{-1}$ s^{-1} independent of temperature (F. L. Nesbitt et al., Temperature dependence of the rate constant for the reaction $F(^2P) + Cl_2 \rightarrow FCl + Cl$ at T = 180–360 K, submitted to *Journal of Physical Chemistry A*, 2003). The $F + Cl_2$ reaction system is ideal for this purpose. There is no complicating secondary

chemistry such as Cl + residual F_2 or F + FCl since these reactions are negligibly slow.

[16] However, these titrations had to be done at temperatures $\geq$180 K. Even though the concentration levels of Cl_2 used here ($[Cl_2] = 2-5 \times 10^{13}$ molecule cm^{-3}) are orders of magnitude below the equilibrium vapor pressure of Cl_2 in the region T = 155–180 K, the Cl_2 signal began decreasing as the temperature of the flow tube decreased below 180 K. When the temperature was then increased above 180 K, the Cl_2 signal returned to its initial value after going through a peak at higher intensity. The validity of the use of the titration results from T = 180–200 K for experiments at T = 155 K was examined by titrating the F-atoms generated from the same initial $[F_2]$ under the same pressure and flow velocity at temperatures of 298 K and 202 K. The same [F] was derived at both temperatures. Therefore the shorter temperature extrapolation from 180–200 K down to 155 K yielded the correct value of the [F].

[17] The initial F atom concentration was determined by measuring the decrease in the Cl_2^+ signal (m/z = 70, electron energy = 14 eV) when the microwave discharge was initiated. The dilute Cl_2/He mixture was admitted to the flow tube via the movable injector. The position of the injector was chosen to ensure that reaction (3) went to completion and that the position was close to the middle of the decay range for the CH_3 reactant. During a previous study [*Cody et al.*, 2002] it was shown that the absolute value of $[F]_0$ was invariant for injector positions of 10 to 40 cm from the sampling pinhole. The absolute F concentration is given by $[F]_0 = [Cl_2]_{\text{disch off}} - [Cl_2]_{\text{disch on}} \equiv \Delta Cl_2$ signal $\times$ $[Cl_2]_{\text{disch off}}$, where ΔCl_2 signal is the fractional decrease in the Cl_2^+ signal, $(S_{\text{dischoff}} - S_{\text{disch on}})/S_{\text{disch off}}$. The uncertainty in $[F]_0$ is estimated to be ±10%. At low $[F]_0$ levels, the procedure was modified as described in the next section.

2.5. MS Scaling Factor for CH_3

[18] The scaling factor for CH_3 is the ratio of the absolute $[CH_3]$ to the mass spectrometer signal at m/z = 15. However, the absolute $[CH_3]$ comes from the F atom titration and hence gives $[CH_3]$ at t = 0 while the mass spectrometer signal is recorded at t $\cong$ 1.5 ms (d $\cong$ 3 cm) and beyond due to the limitation of finite time for mixing at the tip of the injector and perturbations in the flow near the end of the flow tube. For the case of a first order signal decay this is readily handled by a short, linear extrapolation of the signal back to t = 0 in a plot of ln(signal) versus t. This is not an option in the present experiments since the CH_3 signal decay is mostly second order.

[19] We used one of the two procedures adopted in our previous study [*Cody et al.*, 2002] to derive a scaling factor for CH_3. We reduced $[CH_3]$ to the lowest signal level where it was still possible to quantitatively record signal decay. For the present conditions this was $[CH_3] = (2-4) \times 10^{11}$ molecule cm^{-3}. Under these conditions, the methyl signal exhibits apparent first-order decay although modeling shows that there is a substantial second-order component. Thus a plot of ln(methyl signal) versus time appears to be linear and we determine the methyl signal at t = 0 directly by a short linear extrapolation. In our previous work [*Cody et al.*, 2002] we found that the methyl signal at t = 0 was the same within ±10% in both the presence of Cl_2 (where the signal decay is strictly first-order) and in the absence of Cl_2 (where the signal decay appears linear). Addition of Cl_2 in these experiments at T = 155 K was not an option due to loss of Cl_2 at this temperature as described above. At these lower signal levels, the CH_3 background signal was more significant but could be reduced to ~10% of the observed signal as needed by pre-treating the system at room temperature under conditions similar to those employed for the decay of CH_3 in the presence of excess Cl_2 as described previously [*Cody et al.*, 2002].

[20] To relate the signal at t = 0 to $[CH_3]_0$ we need to determine $[F]_0$ at this lower level via the procedure outlined above for higher levels of $[F]_0$. However, determination of the consumption of Cl_2 in the fast titration reaction F + Cl_2 is not straightforward at low levels of [F]. If there is sufficient Cl_2 to ensure complete removal of F by the middle of the CH_3 decay range (d = 20 cm), then the consumption of Cl_2 will be immeasurably small (<1%). By moving the injector out to d = 44 cm, we were able in many instances to achieve essentially complete removal of F. In some instances in which $[Cl_2]$ was rather low, a 10–15% correction for undertitration was made. Separate experiments in our previous work [*Cody et al.*, 2002] showed that, when corrected for undertitration of F by Cl_2, the derived [F] was constant to ±5% between d = 20 and 44 cm.

[21] By combining the CH_3 signal level at t = 0 with the value for $[F]_0$ as determined by F atom titration at the low level of $(2-4) \times 10^{11}$ molecule cm^{-3}, we obtain the desired scaling factor SF = $[CH_3]_0/CH_3$ signal. This scaling factor is then used in the graphical analysis of the $CH_3 + CH_3$ decay experiments at high $[CH_3]$ as described below in section 3. This of course makes the assumption that the scaling factor is the same at both high $[CH_3] = (4-11) \times 10^{12}$ molecule cm^{-3} and low $[CH_3] = (2-4) \times 10^{11}$ molecule cm^{-3}. This requires a linear dependence of signal on concentration, which is inherent in the extraction of a rate constant from the signal decay in this as well as most kinetic experiments and has been well established for mass spectrometric detection.

2.6. Materials

[22] Helium (99.9995%, Air Products) was passed through a trap containing a molecular sieve before entering the flow system or before use in the preparation of mixtures. The molecular sieve was periodically heated to about 220°C under vacuum. F_2 (99.9%, Cryogenic Rare Gases, 5% in He) and CH_4 (99.9995%, MG Industries) were used as provided without further purification. Cl_2 (VLSI 4.8 Grade, Air Products) was degassed at liquid nitrogen temperature.

3. Results

3.1. Experimental Results

[23] Each experiment consisted of two parts: (1) the high methyl decay measurement at $[CH_3] = (4-11) \times 10^{12}$ molecule cm^{-3} to determine the rate constant k_1 and the measurement of $[CH_3]_0$ via F-atom titration with Cl_2; (2) the low methyl decay measurement at $[CH_3] \cong 3 \times 10^{11}$ molecule cm^{-3} to determine the Scaling Factor (SF) along with its F-atom titration to measure $[CH_3]_0$. For one-half of the experiments, the low methyl decay measurement to determine SF was performed both before and after the

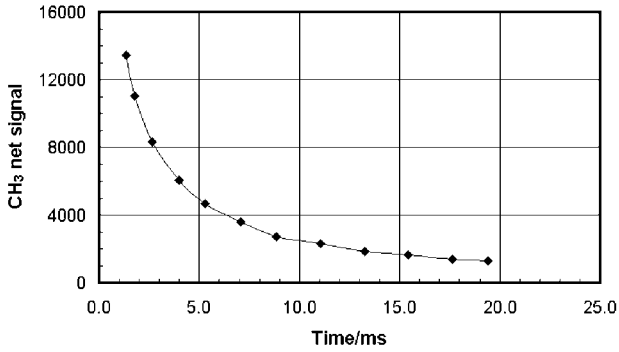

Figure 2. Plot of CH_3 signal versus reaction time at T = 155 K, P = 1.0 Torr He and $[CH_3] = 7.26 \times 10^{12}$ molecule cm^{-3}.

high methyl decay experiment. For the SF determination, the ln (CH_3 signal) versus time was fitted by the linear regression analysis in the Excel spreadsheet program to determine the intercept. The SF is the $[CH_3]_0$ from the titration divided by the intercept.

[24] For the rate constant decay curve at high $[CH_3]$, the inverse of the CH_3 signal versus time was similarly fitted in Excel according to the second order rate equation:

$$1/[CH_3] = 2\,k_1\,t + 1/[CH_3]_0 \qquad (4)$$

Since $[CH_3]$ is the product of the CH_3 signal and the scaling factor SF, this can be written as

$$1/CH_3\ \text{signal} = 2\,k_1\,SF\,t + 1/CH_3\ \text{signal}(t = 0) \qquad (5)$$

[25] Figure 2 shows a typical experimental temporal profile of CH_3 signal at T = 155 K and P = 1 Torr He measured at m/z = 15. The reaction time (t) was derived from the measured distance (x) between the tip of the movable injector to the sampling pinhole and the linear velocity (v) calculated from the measured pressures and gas flows:

$$\text{time(t)} = \text{distance(x)}/\text{velocity(v)} \qquad (6)$$

Figure 3 shows a second order plot of the data displayed in Figure 2. The second order plots using equation (5) were essentially linear. The slopes of these second order plots provided a value for k_1 but the small intercepts were poor estimates of the CH_3 signal at t = 0. This treatment neglects first-order removal of CH_3 via wall loss. However, the rate constant for the first-order wall loss is very small and a temperature independent value $k_{wall} = 10\ s^{-1}$ was estimated from prior work [*Cody et al.*, 2002]. Modeling showed that reaction (1) accounted for >95% of the loss of CH_3 while loss at the wall contributed <5%.

[26] A factor that would adversely affect the CH_3 decay experiments is formation of stabilized but not equilibrated C_2H_6 in Reaction (1) and subsequent dissociative ionization to CH_3^+ in the ionization region. The relative cracking patterns were measured at an I.E. of 15 eV for ethane formed in situ from reaction (1) and then for a comparable concentration of ethane introduced from a 1% C_2H_6 in He mixture. Relative ratios were determined for m/z of 30, 29, 28, and 26 and were the same whether ethane arose from Reaction (1) or from the prepared gas mixture. We thus have no evidence for any contribution from stabilized, non-equilibrated ethane.

[27] At T = 155 K, the rate constant for methyl recombination k_1 was measured at pressures of 0.6, 1.0, and 1.5 Torr He as shown in Table 1. At each pressure, the measured value of k_1 is invariant over approximately a two-fold range of initial methyl concentration. The value of the rate constant is invariant with pressure with k_1(0.6 Torr) = (6.82 ± 2.54) × 10^{-11} cm^3 $molecule^{-1}$ s^{-1}, k_1(1.0 Torr) = (6.98 ± 1.65) × 10^{-11} cm^3 $molecule^{-1}$ s^{-1} and k_1(1.5 Torr) = (6.91 ± 1.47) × 10^{-11} cm^3 $molecule^{-1}$ s^{-1} where the error is 1σ (statistical) + 15% (systematic). The invariance of the rate constant suggests that the reaction is at the high pressure limit in the range P = 0.6–1.5 Torr He. This is not unexpected since we observed [*Cody et al.*, 2002] that, at T = 202 K, our measured value k_1 (2.0 Torr He) = (6.5 ± 1.5) × 10^{-11} cm^3 $molecule^{-1}$ s^{-1} was getting very close to both the experimental value [*Walter et al.*, 1990] of $k_\infty = 6.9 \times 10^{-11}$ cm^3 $molecule^{-1}$ s^{-1} and the calculated values of k_∞ = 6.4 [*Klippenstein and Harding*, 1999], 6.7 [*Hessler and Ogren*, 1996] and 7.1 [*Robertson et al.*, 1995] all in units 10^{-11} cm^3 $molecule^{-1}$ s^{-1}. We therefore take the average of all 23 experiments listed in Table 1 as a measure of the high pressure limit, i.e., $k_\infty = (6.9 \pm 2.0) \times 10^{-11}$ cm^3 $molecule^{-1}$ s^{-1} at T = 155 K. There are no previous experimental measurements of the rate constant at T = 155 K with which our result may be compared. However, there is quite good agreement of our experimental value for k_∞ with the calculated values at T = 155 K of $k_\infty = 7.1 \times 10^{-11}$ cm^3 $molecule^{-1}$ s^{-1} [*Hessler and Ogren*, 1996] and $k_\infty = 7.5 \times 10^{-11}$ cm^3 $molecule^{-1}$ s^{-1} [*Robertson et al.*, 1995].

3.2. Analytical Expression for the Rate Constant

[28] Atmospheric photochemical models require an analytical expression, or at least one that is amenable to numerical computation, for the kinetic rate constant for reaction (1). Ideally, the expression will be valid over the entire range of stratospheric temperatures and pressures where the CH_3 emission originates for the outer planets (T ≈ 120–300 K, P ≈ $1–10^{-5}$ mbar). However, the laboratory results only provide a data table, not an analytical expression, and over a far more limiting range of T and P (see Table 2). We then set out to derive expressions that are consistent with the laboratory data and have some theoretical basis to provide justification for extrapolation.

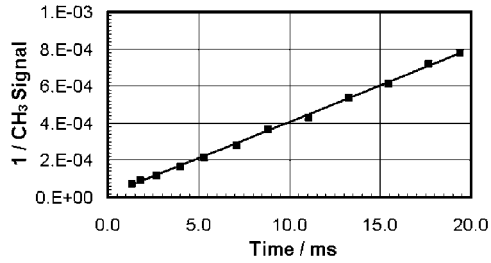

Figure 3. Plot of the reciprocal of the CH_3 signal versus reaction time at T = 155 K, P = 1.0 Torr He and $[CH_3] = 7.26 \times 10^{12}$ molecule cm^{-3}. Data from Figure 2.

Table 1. Summary of Experimental Conditions and Rate Data for the $CH_3 + CH_3$ Reaction at T = 155 K and P = 0.6, 1.0 and 1.5 Torr He

Pressure, Torr	$[CH_3]_0$, 10^{12} molecule cm^{-3}	$[CH_4]_0/[F]_0$	k_1, 10^{-11} cm^3 molecule $^{-1}$ s^{-1}
0.6	10.13	87	6.22
	5.61	159	8.69
	8.45	112	9.26
	6.66	134	8.16
	7.37	128	5.83
	7.57	130	5.08
	8.67	113	5.33
	5.52	180	6.03
			< 6.82 ± 2.54 >[a]
1.0	9.08	95	6.95
	4.54	192	7.32
	10.82	80	6.97
	7.58	115	5.91
	6.83	127	7.15
	5.50	176	7.22
	7.99	122	7.41
	8.44	109	6.67
	6.52	138	5.76
	7.26	122	6.89
	4.55	193	7.48
	8.08	110	7.98
			< 6.98 ± 1.65 >[a]
1.5	7.60	131	7.50
	4.89	189	6.78
	9.30	103	6.46
			< 6.91 ± 1.47 >[a]

[a]Mean central value of k_1 at each pressure; error is one standard deviation ($\pm 1\sigma$) plus an additional 15% for systematic errors.

[29] Ethane produced by the combination of methyl radicals in reaction (1) has a minimum internal energy, E_0, equal to the bond dissociation energy of the formed carbon-carbon bond. The internal thermal energy carried by the methyl radicals and the kinetic energy of the collision is added to this minimum energy. Thus the ethane formed by the combination reaction has a somewhat distorted Boltzmann internal energy distribution which is zero below E_o and a convolution of energy modes above E_o. However, for this discussion we will use the average of the internal energy E_{th}. As long as the internal energy of ethane is greater than E_o then it will decompose by breaking the carbon-carbon bond that was initially formed. The amount of decomposition (D) will quantitatively reduce the apparent rate constant for the combination reaction. The internal energy can be removed by photon emission or collisional stabilization; the yields for these processes are P and S, respectively. For further simplification we have assumed that the energy removed by photon emission or collisional stabilization is equal to or greater than E_{th}. Thus by conservation of mass the nascent ethane formed by combination of methyl radicals will be distributed between S and D. Photon emission will also occur at energies less than the reaction threshold and in general will involve sequential steps. The simplest model would have either a single emission or collision removing sufficient energy so that nascent ethane would not decompose. Weak collision calculations do not include this constraint.

[30] The fraction of nascent ethane formed by methyl radical combination, (P + S)/(P + S + D), is determined by the competition between D, P and S. The apparent second order rate constant for combination is the product of the rate constant for the bimolecular encounter frequency (k_c) for methyl radicals times the fraction stabilized:

$$k = k_c(P + S)/(P + S + D) \quad (7)$$

Three pressure regimes can be considered:

[31] P > S: At very low pressure photon stabilization is the dominant path for stabilization, i.e., P + D > S, and $k = k_c P/(P + D)$ is a constant independent of pressure.

[32] S > P: At moderate pressures bimolecular collisions are the dominant stabilization path, i.e., S > P, and $k = k_c S/(S + D)$ is pressure dependent. For $D \gg S$ the reaction becomes termolecular.

[33] S > (P + D): In the high-pressure limit all the formed ethane is stabilized and $k = k_c$ and the reaction becomes bimolecular.

[34] Calculations have been reported [*So and Dunbar*, 1989] for photon cooling of vibrationally excited benzene; the rate coefficient is <2 s^{-1}. Assuming that the radiative cooling for ethane is comparable to that for benzene, then for P > S the pressure must be $<10^{-7}$ mbar. Although these pressures do occur in the atmospheres of Neptune and Saturn they are much lower than those present at the altitudes where the CH_3 emission originates ($P > 10^{-5}$ mbar). Thus photon stabilization does not have to be included in the modeling of the pressure dependence of the combination of methyl radicals.

[35] Using detailed balance it can be shown that the rate coefficient for combination is proportional to the unimolecular rate constant for decomposition of the combination product [*Smith and Gilbert*, 1990]. The primary extension of the "2" level scheme of *Lindemann* [1922] and *Hinshelwood* [1940], hereafter referred to simply as the Lindemann scheme or expression, is easily expanded to include all energies which can react. Models have been fully developed [*Holbrook et al.*, 1996; *Forst*, 1973] which describe the unimolecular decomposition, i.e., competition between D and S, at the molecular level. RRKM theory is used to compute the microscopic rate constants for decomposition, k_E [*Marcus and Rice*, 1951; *Marcus*, 1952]. Observed

Table 2. Summary of Measured Rate Constants for $CH_3 + CH_3$ for T $\leq$ 298 K and He Bath Gas

Temperature, K	Pressure, Torr	[He], molecule cm^{-3}	k, cm^3 molecule^{-1} s^{-1}	References[a]
298	1.0	3.2×10^{16}	$(3.5 \pm 0.5) \times 10^{-11}$	4
298	1.0	3.2×10^{16}	$(2.9 \pm 0.8) \times 10^{-11}$	5
298	0.55	1.8×10^{16}	$(1.8 \pm 0.7) \times 10^{-11}$	5
298	1.0	3.2×10^{16}	$(2.4 \pm 0.5) \times 10^{-11}$	1
298	0.6	1.9×10^{16}	$(2.1 \pm 0.4) \times 10^{-11}$	1
296	10.5	34.3×10^{16}	$(3.7 \pm 0.7) \times 10^{-11}$	2
296	5.2	16.8×10^{16}	$(3.7 \pm 0.7) \times 10^{-11}$	2
296	2.4	7.9×10^{16}	$(3.6 \pm 0.7) \times 10^{-11}$	2
202	2.0	9.6×10^{16}	$(6.5 \pm 1.5) \times 10^{-11}$	1
202	1.0	4.8×10^{16}	$(5.2 \pm 1.4) \times 10^{-11}$	1
202	0.6	2.9×10^{16}	$(5.0 \pm 1.1) \times 10^{-11}$	1
155	1.5	9.3×10^{16}	$(6.9 \pm 1.5) \times 10^{-11}$	3
155	1.0	6.2×10^{16}	$(7.0 \pm 1.6) \times 10^{-11}$	3
155	0.6	3.7×10^{16}	$(6.8 \pm 2.5) \times 10^{-11}$	3

[a]References: 1, *Cody et al.* [2002]. 2, *Slagle et al.* [1988]. Error bars were calculated using their statement that "the measured values of k are estimated to have a most probable accuracy of ±20%." 3, this work. 4, *Stoliarov et al.* [2000]. 5, *Deters et al.* [1998a, 1998b].

Table 3. Summary of k_0 Derived from Laboratory Data Assuming k_∞ as Given by *Hessler* [1997]

T, K	P, Torr	[He], molecule cm^{-3}	Calculated k_0, cm^6 $molecule^{-2}$ s^{-1}	References[a]
298	10.6[b]	34.3×10^{16}	2.87×10^{-28}	2
298	5.2[b]	16.8×10^{16}	5.97×10^{-28}	2
298	2.4[b]	7.9×10^{16}	1.16×10^{-27}	2
298	1.0	3.2×10^{16}	2.64×10^{-27}	4
298	1.0	3.2×10^{16}	1.75×10^{-27}	5
298	1.0	3.2×10^{16}	1.28×10^{-27}	1
298	0.6	1.9×10^{16}	1.74×10^{-27}	1
298	0.55	1.8×10^{16}	1.45×10^{-27}	5
202	2.0	9.6×10^{16}	1.41×10^{-26}	1
202	1.0	4.8×10^{16}	4.70×10^{-27}	1
202	0.6	2.9×10^{16}	6.64×10^{-27}	1
155	1.5	9.3×10^{16}	1.18×10^{-26}	3
155	1.0	6.2×10^{16}	2.30×10^{-26}	3
155	0.6	3.7×10^{16}	2.39×10^{-26}	3

[a]References: 1, *Cody et al.* [2002]; 2, *Slagle et al.* [1988]; 3, this work; 4, *Stoliarov et al.* [2000]; 5, *Deters et al.* [1998a, 1998b].

[b]The *Slagle et al.* [1988] data were taken at T = 296K. We assume that k(298) ≅ k(296) and recalculate P for T = 298K.

macroscopic rate constants are computed by solving the master equation using the k_E's, collision frequency and collisional energy transfer probabilities as input [*Tardy and Rabinovitch*, 1977; *Oref and Tardy*, 1990]. There is good agreement between the calculated and experimental results for many systems. The lack of information on the temperature dependence of the collision frequency and energy transfer probabilities has hampered the comparison of calculations and experiments at lower temperatures.

[36] Although definitive master equation calculations are affordable on present desktop computers, models that parameterize the pressure and temperature dependencies are often used in simulating atmospheric systems. Such models which extend the Lindemann scheme have been developed by Troe [*Troe*, 1977a, 1977b, 1979; *Gilbert et al.*, 1983] and Oref [*Oref*, 1989; *Pawlowska and Oref*, 1990]. Two necessary quantities are k_0, the limiting low pressure (or termolecular) rate constant in units of cm^6 $molecule^{-2}$ s^{-1}, and k_∞, the limiting high-pressure (or bimolecular) rate constant in units of cm^3 $molecules^{-1}$ s^{-1}. Other parameters are often used to account for the range of energies associated with the decomposition, e.g., amount of energy transferred, anharmonicity, etc. The temperature dependence of these parameters is also often parameterized. Thus fall-off curves, the decline of the rate constant with decreasing pressure, can be rapidly calculated. In most cases these models have been successfully used for unimolecular and combination reactions for temperatures greater than 300 K; there are some systems where successful models have been achieved for lower temperatures. The major problem with extrapolating these models to low temperature is that ''calibration'' or validity of the model frequently can not be tested or compared to experiment.

3.2.1. Lindemann Expression

[37] The expression for the combination (bimolecular) reaction taken from the Lindemann scheme is

$$k = \frac{k_0 k_\infty [M]}{k_0 [M] + k_\infty} \tag{8}$$

where $[M]$ is the number density in molecules cm^{-3}, and k, k_0 and k_∞ are as before. Note that k, the overall rate constant, is a bimolecular rate constant with units of cm^3 $molecules^{-1}$ s^{-1}. In equation (8) the pressure dependence of k comes from the functional relationship among k_0 and k_∞ and $[M]$ while the temperature dependence of k comes about via the temperature dependence of k_0 and k_∞ themselves. In principle, a least squares technique could be used to determine k_0 and k_∞ from equation (8) at the four temperatures (T = 298 K, 296 K, 202 K and 155 K) listed in Table 2. Once k_0 and k_∞ are known at this set of temperatures we can then determine their temperature dependencies, and then both the pressure and temperature dependence of k is known and can be used in the photochemical models.

[38] The usefulness of the T = 155K data set was limited because normal experimental error requires the measurement of k deep into the fall-off so that errors in k_0 can be minimized. In addition, the T = 298 K and 296 K measurements represent a single temperature because the T = 296 K data are near the high-pressure regime and because of the weak temperature dependence of k_∞. Furthermore not all of the T = 298K data are equal; the *Stoliarov et al.* [2000] and *Deters et al.* [1998a, 1998b] values for the $CH_3 + CH_3$ reaction rate constant were by-products of more extensive studies of the reaction of CH_3 with other free radicals. We experimented with various groupings of the T = 298K data to determine which set of studies produced the best k_0 and k_∞ values as determined by a minimum in χ^2 and a linear correlation coefficient nearest unity. It was not possible to distinguish a single best set so instead we focused on bounding the value of k_0 at T = 298 K, i.e., a set that produced the lowest possible value of k_0, a middle value, and the highest possible value.

[39] When we derived both k_0 and k_∞ from the data, the derived k_∞ was found to be compatible (<10% difference) with that predicted by *Hessler* [1997]:

$$k_\infty = 9.3132 \times 10^{-11} e^{-1.519 \times 10^{-3} \times T} \tag{9}$$

This expression was derived from data in the temperature range 200–906K. Since there is theoretical support for this expression and it matches the data, it satisfies our two criteria above. Note that with this expression k_∞ increases weakly with decreasing temperature. Equation (9) was then adopted as an expression for the temperature dependence of k_∞.

[40] With k_∞ now known, we then used equation (8) to derive only k_0 from the laboratory data summarized in Table 2. The results are shown in Table 3. As can be seen in Table 3 k_0, like k_∞, increases with decreasing temperature. Comparison in Table 3 of k_0 retrieved from the low and high-pressure laboratory T = 298 K data [*Cody et al.*, 2002; *Slagle et al.*, 1988] shows the danger of trying to retrieve k_0 in the high-pressure regime. The values of k_0 derived from the T = 155 K data should be treated as lower limits.

[41] With values for k_0 at three different temperatures, we then curve fit an expression of k_0 to this data assuming one of two functional forms for the temperature dependence. Either an Arrhenius type expression:

$$k_0 = A e^{\left(-B/T\right)} \tag{10}$$

Table 4. Summary of Terms A, B, and n in Expressions for k_0 in He Derived From Laboratory Data Assuming k_∞ as Given by *Hessler* [1997]

Case[a]	A[b]	B[b]	n[b]	References[c,d]
i	1.15×10^{-29}	−1334.	n/a	1 and 2
ii	4.34×10^{-29}	−1066	n/a	1, 2, and 5
iii	8.03×10^{-29}	−941.3	n/a	1 and 4
iv	1.64×10^{-28}	−757.4	n/a	1, 3, and 4
v	1.646×10^{-4}	985.4	−8.749	1, 2, 3, 4, and 5

[a]Cases i-iv assume k_0 as defined by equation (10) and k as defined by equation (8) in the text. Similarly, case v employs equations (11) and (8).
[b]Terms A, B, and n given in equations (10) or (11) in the text.
[c]Fit to average of k_0 retrieved from the data in the indicated references.
[d]References: 1, *Cody et al.* [2002]; 2, *Slagle et al.* [1988]; 3, this work; 4, *Stoliarov et al.* [2000]; 5, *Deters et al.* [1998a, 1998b].

or a Transition-State theory type expression:

$$k_0 = AT^n e^{\left(-B/T\right)} \tag{11}$$

For the Arrhenius type expression, we have two unknowns (*A* and *B*) but three data sets; thus a least squares fitting routine was used. Because of the limitations of the high-pressure T = 298 K data and the T = 155 K data discussed above, we retrieved a set of Arrhenius type expressions depending on which data were included in the least squares fitting routine with the intention of bounding the temperature dependence of k_0. For the Transition-State theory expression, the number of unknowns is the same as the number of data sets; thus *A*, *B*, and *n* can be retrieved exactly from the data. Results are summarized in Table 4 and sample comparisons of expressions to data are shown in Figures 4–7.

[42] As Figures 4–7 illustrate, it is not possible to select one of these 5 expressions as best fitting the laboratory data. For the two parameter fits, i.e., the Arrhenius expression, the data limit the range of values of *A* and *B* that are consistent with the data (see Table 4). However, the values of A and B are correlated in the sense that the quality of the fit of equation (10) to a data set remains close to optimum when both A and B are increased or decreased. All of the Arrhenius expressions have k_0 monotonically increasing for decreasing temperature. This is not the case for the Transition-State theory type expression, i.e., case v. For this expression k_0 starts to decrease with decreasing temperature at T = 112 K. Since this behavior is not expected theoretically, we take T = 112 K as the lower limit to which our Transition-State theory type expressions for k_0 is valid. Note that this turn around behavior, k_0 decreasing with decreasing temperature, also occurs for the Transition-State theory expressions of k_0 from *Baulch et al.* [1992] and *Slagle et al.* [1988] but at a higher temperature, T = 198–197 K. For the modeling of $CH_3 + CH_3$ reaction on the outer planets, the reaction is in the high pressure regime at T = 112 K while at T = 198 K it is in the low pressure regime. Thus where our Transition-State theory expression for k_0 fails we are in the high-pressure limit of the reaction and it is not a problem. This is not the case for the expressions from *Baulch et al.* [1992] and *Slagle et al.* [1988].

3.2.2. Oref's Extension of the Lindemann Scheme

[43] The Lindemann "2 state" model is an over simplification of real systems. Various extensions of this model have been suggested. The basic idea is to parameterize the simplified model by using the low and high pressure limiting rate constants (k_0 and k_∞) and shape factors. The advantage of such parameterization is that complete fall off curves can be found at any temperature without resorting to time intensive master equation calculations. In the present work we have used Oref's Extension of the Lindemann Scheme. Oref's [*Oref*, 1989; *Pawlowska and Oref*, 1990] model is based on the behavior for a multistate Lindemann model and a $J_{3/2}$ term is introduced. The terminology used here is based on the combination reaction and has been

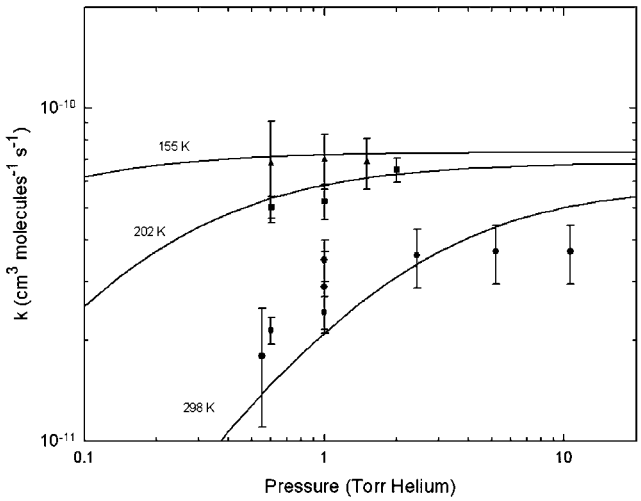

Figure 4. Comparison of derived analytical expression for $CH_3 + CH_3$ to laboratory data. The laboratory data (with error bars) are shown as individual points: circles are T = 298 K data, squares are T = 202 K data, and triangles are T = 155 K data. See Table 2 for details. Solid curves labeled with a temperature are the calculated rate constant as a function of pressure for the three temperatures. The curves were generated using the parameters and formula given in Table 4 for Case i.

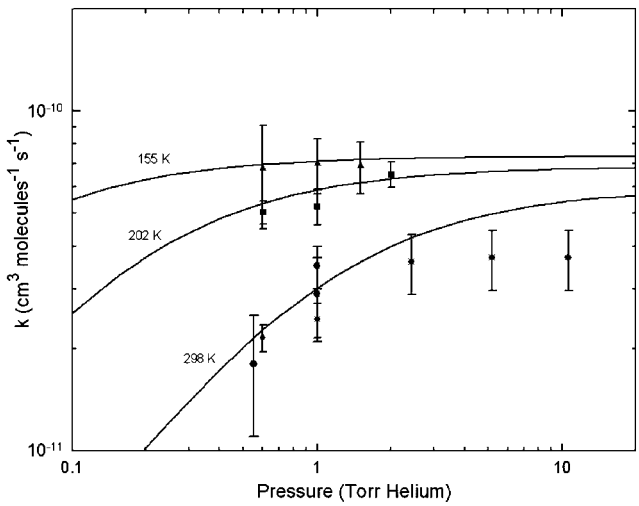

Figure 5. Same as Figure 4 except the curves were generated using the parameters and formulas given in Table 4 for Case iii.

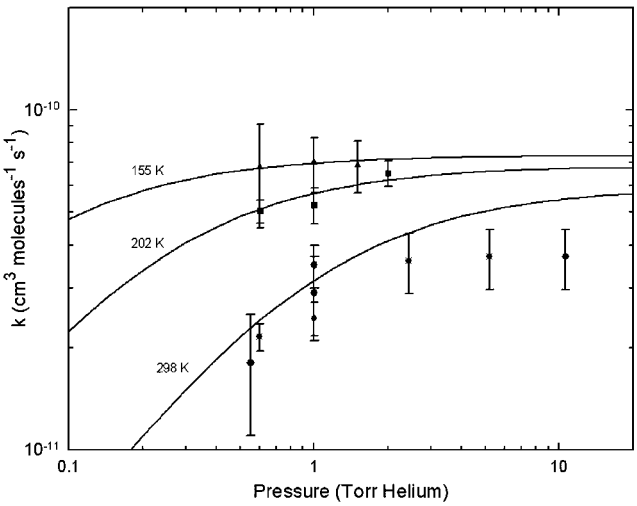

Figure 6. Same as Figure 4 except the curves were generated using the parameters and formulas given in Table 4 for Case iv.

translated from the context of a unimolecular reaction that was reported by Oref. The $J_{3/2}$ term for the unimolecular reaction relates to the reaction order being half way between 1 and 2, i.e., 3/2. For the combination reaction $J_{3/2}$ becomes $J_{5/2}$ since the reaction order goes from 2 (high-pressure limit) to 3 (low-pressure limit). Thus the Oref expression for calculating k is

$$k = \frac{-(k_\infty + k_0\ M) + \sqrt{(k_\infty + k_0\ M)^2 + 4(J_{5/2} - 1)k_\infty\ k_0\ M}}{2(J_{5/2} - 1)} \tag{12}$$

where k_0 and k_∞ are as before. $J_{5/2}$ is calculated from the expression

$$J_{5/2} = \left[k_\infty / k_{5/2} - 1\right]^2$$

where $k_{5/2}$ is the rate constant when the reaction is 5/2 order. An increase in $J_{5/2}$ broadens the falloff region and is equivalent to an increasing value of F in Troe's extension (see section 4.1).

[44] To determine k_0, k_∞ and $J_{5/2}$ we proceeded as follows. Values of k_0, k_∞, and $J_{5/2}$ were determined that best fit the calculations of *Klippenstein and Harding* [1999] (argon bath gas) at T = 200 K, 296 K, and 407 K. Since k_∞ is independent of bath gas we can use it without modification. Since k_0 is proportional to the collision frequency, we calculate k_0 for helium by converting the k_0 calculated by *Klippenstein and Harding* [1999] for argon by using the appropriate reduced masses and Lennard-Jones collision cross sections (see Troe references for details). For the same energy removed per collision, at the same pressure, He is found to be 80% as effective as Ar in stabilizing the hot C_2H_6 adduct; the smaller cross section for helium is nearly compensated by its lighter mass and hence a larger relative velocity. The results are presented in Table 5. We then assumed that the temperature dependence of k_0 and k_∞ could be adequately described by an Arrhenius expression. We determined the A and B parameters by using a least squares routine. The temperature dependence of $J_{5/2}$ is more complicated. For low temperatures, $J_{5/2}$ approaches an asymptotic value, a little greater than one. $J_{5/2}$ cannot equal one since the above expression for k (equation (12)) then goes to infinity. For higher temperatures, $J_{5/2}$ is expected to vary as

$$\sqrt{J_{5/2}} + 1 = A\ e^{-B/T} \tag{13}$$

However a simple Arrhenius expression fits our limited set of J values better and was therefore adopted. Our derived temperature dependent expressions are then

$$k_0 = 5.822 \times 10^{-28}\ e^{564.54/T}$$

$$k_\infty = 4.504 \times 10^{-11} e^{70.12/T} \tag{14}$$

$$J_{5/2} = 163 \times e^{-1001/T},\ \textit{If}\ \left(J_{5/2} \leq 1.1\right)\ \textit{then}\ J_{5/2} = 1.1$$

The predicted k from equation (12), using the expressions of equation (14), is then compared to the data in Figure 8.

[45] However, the information in Tables 4 and 5, and equations (8), (9), (10), (11), (12), and (14) all relate to k in He as a bath gas, while the background atmospheres for the outer planets are $\approx$ 90% H_2 and only 10% He. While the bath gas does not have an effect on k_∞ (all excited C_2H_6 is stabilized), it does have an effect on k_0. The magnitude of k_0 is a function of the intrinsic collisional efficiency, the collision cross section and the reduced mass of the collision partners. The intrinsic efficiency for hydrogen and helium are nearly identical. However the difference in the reduced mass and collision cross sections for the collision with ethane requires that $k_0(H_2)/k_0(He)$ = 1.78 and 1.72 at T = 202 and 296 K, respectively. Thus, for the same pressure (in the low-pressure linear region) at T = 202 K, a hydrogen atmosphere will have a k_0 about 1.8 times larger than that for helium. Since we are interested in calculating the rate constant for the

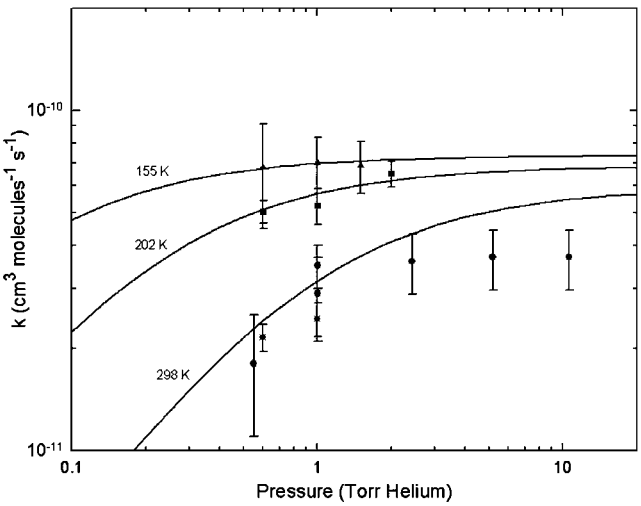

Figure 7. Same as Figure 4 except the curves were generated using the parameters and formulas given in Table 4 for Case v.

Table 5. Values for k_0, k_∞, and $J_{5/2}$ Derived From *Klippenstein and Harding* [1999] Modified for He[a]

T, K	k_0, cm^6 molecule^{-2} s^{-1}	k_∞, cm^3 molecule^{-1} s^{-1}	$J_{5/2}$
200	8.88×10^{-27}	6.32×10^{-11}	1.10
296	5.13×10^{-27}	5.90×10^{-11}	5.43
407	1.96×10^{-27}	5.24×10^{-11}	14.10

[a]The overall rate constant is of the form $k = \frac{-(k_\infty + k_0 M) + \sqrt{(k_\infty + k_0 M)^2 + 4(J_{5/2} - 1) k_\infty \; k_0 \; M}}{2(J_{5/2} - 1)}$.

outer planets, we multiplied our k_0 derived from the He lab data (Tables 3 and 5) by 1.8 and derived a new set of analytical expressions with parameters given in Table 6 for the Lindemann expressions and for Oref as

$$k_0 = 9.682 \times 10^{-28} e^{569.4/T}$$

$$k_\infty = 4.504 \times 10^{-11} e^{70.12/T} \tag{15}$$

$$J_{5/2} = 163 \times e^{-1001/T}, \;\; If\left(J_{5/2} \leq 1.1\right) \; then \; J_{5/2} = 1.1.$$

4. Photochemical Modeling

4.1. Review and Comparison of Laboratory Data to Previous Models

[46] Several recent papers have attempted to analyze the CH_3 emission seen on Saturn and Neptune by using the results from 1-D photochemical models [*Bézard et al.*, 1998, 1999; *Moses et al.*, 2000; *Lee et al.*, 2000]. The primary source of CH_3 in the stratospheres on the outer planets is methane photolysis either directly or indirectly:

$$CH_4 + h\nu \rightarrow CH_3 + H \tag{16}$$

$$CH_4 + h\nu \rightarrow {}^1CH_2 + H_2 \tag{17}$$

$${}^1CH_2 + H_2 \rightarrow CH_3 + H \tag{18}$$

and the primary sink is recombination to form C_2H_6:

$$CH_3 + CH_3 + M \rightarrow C_2H_6 + M \tag{1}$$

Other important sources and sinks for CH_3 are shown in Figure 9. The pressure level at which this photochemistry occurs is controlled by how well the atmosphere is mixed. Methane is the primary reservoir for carbon in the upper tropospheres of these planets. It is transported upward into the stratospheres to replace the methane that is lost via photolysis. Since methane is much heavier than the background atmospheric species (H_2 and He), it is only present at pressures where the mixing time is shorter than the diffusive separation time. In 1-D photochemical models the strength of vertical transport/mixing is parameterized via the eddy diffusion coefficient K. This represents the strength of vertical mixing in the atmosphere independent of its source: small scale eddies, large scale eddies, or mass motion that result in overturning of the atmosphere. Higher values of *K* represent stronger vertical mixing and results in CH_4 photolysis occurring at lower pressures. With the exception of Uranus, the changeover from a well-mixed atmosphere to one which is diffusively separated occurs at $P \leq 10^{-3}$ mbar (1 microbar). This means that on all of these planets CH_3 recombination occurs in the low-pressure regime of the reaction where the reaction rate constant is not only temperature dependent but also pressure dependent. Thus the model-predicted CH_3 abundance is sensitive to both the $CH_3 + CH_3$ recombination rate constant and the value and altitude profile of K.

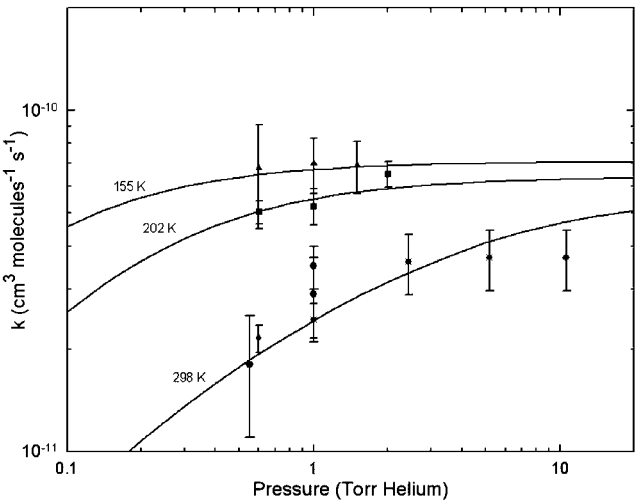

Figure 8. Same as Figure 4 except the curves were generated using the parameters and formulas given in equations (12) and (14).

[47] Unfortunately the altitude profile of K can be parameterized in many different ways [e.g., see *Hunten*, 1975; *Romani et al.*, 1993; *Bishop et al.*, 1995; *Moses et al.*, 2000] adding to the complexity of sorting out k versus K differences. To bound this large parameter space, we have chosen to limit our selection of K and its profile to those used in the previous studies of CH_3 emission on Saturn and Neptune. This is consistent with our goal to see if the rate constant expressions for $CH_3 + CH_3$ in H_2 derived here from our and other low temperature laboratory data affect the conclusions of these papers: that an increase in this rate constant would allow K derived from the CH_3 studies to be consistent with K derived from other techniques, notably model-observation comparisons of the other hydrocarbon

Table 6. Summary of Terms A, B, and n in Expressions for k_0 in H_2 Derived From Laboratory Data Assuming k_∞ as Given by *Hessler* [1997]

Case[a]	A[b]	B[b]	n[b]	References[c,d]
i	1.97×10^{-29}	−1332.	n/a	1 and 2
ii	4.91×10^{-29}	−1066	n/a	1, 2, and 5
iii	1.36×10^{-28}	−941.2	n/a	1 and 4
iv	2.78×10^{-28}	−757.5	n/a	1, 3, and 4
v	2.666×10^{-4}	983.8	−8.742	1, 2, 3, 4, and 5

[a]Cases i-iv assume k_0 as defined by equation (10) and k as defined by equation (8) in the text. Similarly, case v employs equations (11) and (8).
[b]Terms A, B, and n given in equations (10) or (11) in the text.
[c]Fit to average of k_0 retrieved from the data in the indicated references.
[d]References: 1, *Cody et al.* [2002]; 2, *Slagle et al.* [1988]; 3, this work; 4, *Stoliarov et al.* [2000]; 5, *Deters et al.* [1998a, 1998b].

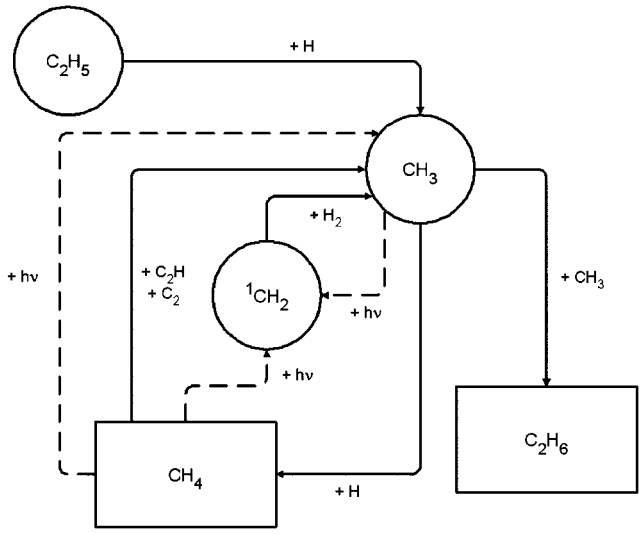

Figure 9. Major sources and sinks for CH_3 in the stratospheres of the outer planets. Rectangles denote stable species, circles are free radicals, solid lines are chemical reactions, and dashed lines are photolytic pathways.

species and CH_4 in particular. We used two different types of K profiles. The first is the commonly used profile of $K \propto M^{-1/2}$, where M is the atmospheric number density. *Bézard et al.* [1998], *Bézard et al.* [1999], *Moses et al.* [2000] and *Lee et al.* [2000] used a similar profile, albeit steeper than $M^{-1/2}$. The values of K we used with this type of profile are shown in Tables 7 and 8. For D, the methane molecular diffusion coefficient, we used the parameters and expression given in Table 9. For Neptune, *Bézard et al.* [1999] and *Lee et al.* [2000] used a quite different K profile, one similar to the Case B type profile of *Romani et al.* [1993] with

$$K = 2.0 \times 10^3 \text{ cm}^2 \text{ sec}^{-1} \text{ for P} > 2 \text{ mbar}$$

$$\text{Rapid increase for 2 mbar} > P > 0.5 \text{ mbar}$$

$$K = 5.0 \times 10^7 \text{ cm}^2 \text{ sec}^{-1} \text{ for 0.5 mbar} > P > 5 \times 10^{-3} \text{ mbar}$$

$$\text{Rapid decrease for } 5 \times 10^{-3} \text{ mbar} > P > 8 \times 10^{-4} \text{ mbar}$$

$$K = 1.0 \times 10^5 \text{ cm}^2 \text{ sec}^{-1} \text{ for P}$$

Therefore we investigated the effect of that type of *K* profile for Neptune.

Table 7. Parameters and Values for K in Saturn's Atmosphere[a]

C	K_t, cm^2 s^{-1}	K_h, cm^2 s^{-1}
3.77×10^{13}	1.63×10^4	10^8
2.51×10^{13}	1.09×10^4	5×10^7
1.45×10^{13}	6.26×10^3	2×10^7
1.02×10^{13}	4.41×10^3	10^7
7.15×10^{12}	3.10×10^3	5×10^6
4.58×10^{12}	1.98×10^3	2×10^6

[a]K is the eddy diffusion coefficient in units of cm^2 s^{-1} and is given by $K = C \times M^{-1/2}$, where C is the proportionality constant and M is the atmospheric number density in molecules cm^{-3}. K_t is the value at the tropopause (P = 60.4 mbar, T = 82 K), and K_h is the value at the methane homopause (defined to be where K = D, the methane molecular diffusion coefficient in the background atmosphere).

Table 8. Parameters and Values for K in Neptune's Atmosphere[a]

C	K_t, cm^2 s^{-1}	K_h, cm^2 s^{-1}
1.26×10^{13}	5.47×10^3	10^7
8.75×10^{12}	3.79×10^3	5×10^6
5.15×10^{12}	2.23×10^3	2×10^6

[a]K is the eddy diffusion coefficient in units of cm^2 s^{-1} and is given by $K = C \times M^{-1/2}$, where C is the proportionality constant and M is the atmospheric number density in molecules cm^{-3}. K_t is the value at the tropopause (P = 115 mbar, T = 53 K), and K_h is the value at the methane homopause (defined to be where K = D, the methane molecular diffusion coefficient in the background atmosphere).

[48] Lastly, in all of these papers, k_0 is based on laboratory data with Ar as the bath gas. To compare the rate constant expressions used in these papers to our He laboratory data we first converted their k'_0s to be applicable to our He data by multiplying them by 0.8 for the same reasons given previously. We now review these photochemical modeling papers in chronological order.

[49] *Bézard et al.* [1998] noted that while their standard photochemical model worked well to explain the observations of CH_4 and the C_2 hydrocarbons on Saturn, it overestimated the CH_3 emission by a factor of 6. They looked at two different solutions to this problem. The first was to lower the value of the eddy diffusion coefficient in the upper atmosphere of Saturn. This increases the pressure where the CH_3 is formed and thus increases the CH_3 sink via the pressure dependence of the CH_3 recombination rate. They found that they had to lower K_h by almost 2 orders of magnitude, from 6×10^7 cm^2 sec^{-1} to 7×10^5 cm^2 sec^{-1}, to match the CH_3 observations. K_h is the eddy diffusion coefficient at the methane homopause, defined to be where K = D, the methane molecular diffusion coefficient in the atmosphere. However, this resulted in the model no longer being able to fit the CH_4 observations. They then looked at the low-pressure rate for CH_3 recombination used in their model. Their standard model used the *Slagle et al.* [1988] expression for k_0:

$$k_0 = 8.77 \times 10^{-7}\ T^{-7.03} e^{\left(-1390/T\right)} \tag{19}$$

and k_∞ from *Baulch et al.* [1992]

$$k_\infty = 6.0 \times 10^{-11} \tag{20}$$

Table 9. Parameters for Calculating the CH_4 Molecular Diffusion Coefficient[a]

Bath Gas	A	s
H_2	2.3×10^{17}	0.765
He	2.3×10^{17}	0.750

[a]The methane molecular diffusion coefficient in units of cm^2 s^{-1} in the specified bath gas is given by $D_{H2 \text{ or } He} = (A \times T^s)/M$, where T is the temperature in K and M is the atmospheric number density in molecules cm^{-3}. The effective methane molecular diffusion coefficient in the background atmosphere is given by $D = \frac{1}{\left(f_{H2}/D_{H2} + f_{He}/D_{He}\right)}$, where f_{H2} is the mixing ratio of H_2, and similarly for f_{He} for He [*Marrero and Mason*, 1972].

They observed that the use of k_0 based on the laboratory work of *Macpherson et al.* [1983]

$$k_0 = 6.0 \times 10^{-29} e^{1680/T} \quad (21)$$

resulted in a larger k_0 (factor of 280) at T = 140 K (a typical temperature in the upper atmosphere of Saturn) compared to use of the data of *Slagle et al* [1988]. However, in both cases, k_0 is based on measurements for $T \geq 296$ K and Ar as a bath gas. With the use of k_0 based on the *Macpherson et al.* [1983] paper they were then able to reproduce the observed CH_3 emission without lowering the eddy diffusion coefficient. *Moses et al.* [2000] essentially confirmed this work with $K_h = 1.7 \times 10^7$ cm^2 sec^{-1} if k_0 from *Macpherson et al.* [1983] was used and $K_h = 7 \times 10^5$ cm^2 sec^{-1} if k_0 from *Slagle et al.* [1988] was used. *Moses et al.* [2000] also includes a discussion on K_h derived from other studies compared to K_h derived from model-observation comparison for CH_3. All of these studies, with the exception of one that can be explained by the different choice of the altitude profile of K (*Smith et al.* [1983] assumed K constant with height and derived $K_h = 5 \times 10^6$ cm^2 sec^{-1}), derive a higher K_h than that derived from model-observation comparison of the CH_3 emission if k_0 from *Slagle et al.* [1988] is used: $K_h = (4 \pm 1) \times 10^7$ cm^2 sec^{-1} [*Drossart et al.*, 1999]; $K_h = (8 \pm 4) \times 10^7$ cm^2 sec^{-1} [*Sandel et al.*, 1982]; $K_h = (1.7 + 0.4/-0.1) \times 10^8$ cm^2 sec^{-1} [*Atreya*, 1982]; $K_h > 10^9$ cm^2 sec^{-1} [*Parkinson et al.*, 1999].

[50] In Figure 10 we compare k calculated by using the parameters given by *Bézard et al.* [1998], k_0 from *Macpherson et al.* [1983] corrected for He and k_∞ from *Baulch et al.* [1992], to the laboratory data. Of all three temperatures, the expression used by *Bézard et al.* [1998], matches the data best at T = 155 K. However, the use of the larger k_0 has the effect of predicting that the reaction stays in the high pressure regime at lower pressures at T = 202 K and 298 K than is supported by the laboratory data. We feel that any of our above expressions for k better reproduces the laboratory data.

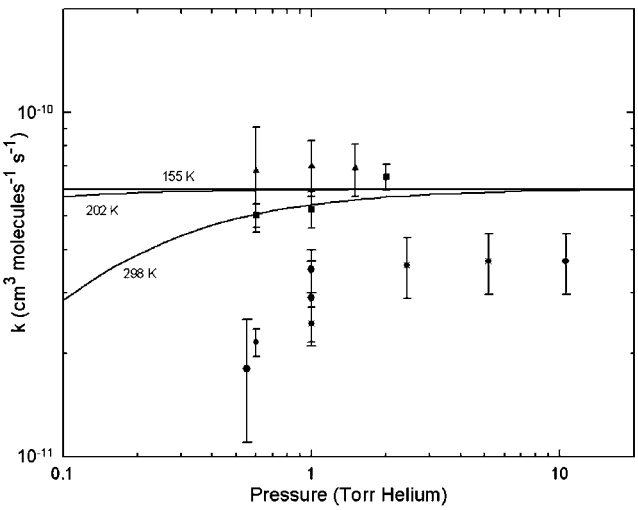

Figure 10. Same as Figure 4 except the curves were generated using the parameters and formulas given by *Bézard et al.* [1998], k_0 from *Macpherson et al.* [1983] corrected for He and k_∞ from *Baulch et al.* [1992], to model CH_3 emission from Saturn.

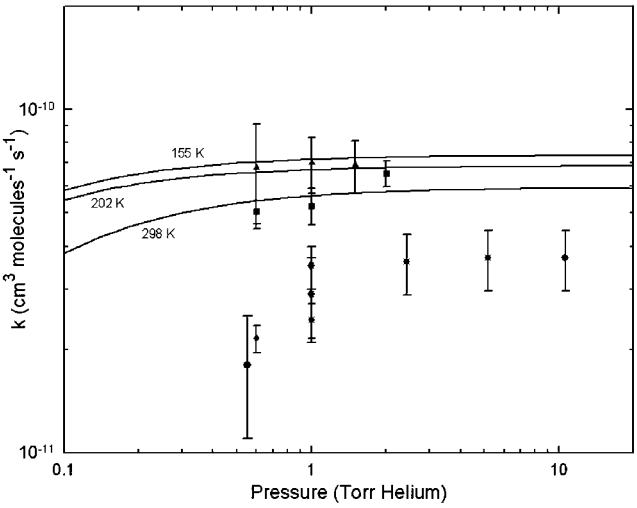

Figure 11. Same as Figure 4 except the curves were generated using the parameters and formulas given by *Bézard et al.* [1999], k_0 from *Slagle et al.* [1988] corrected for He and k_∞ from *Hessler* [1997], to model CH_3 emission from Neptune.

[51] *Bézard et al.* [1999] ran into a similar problem on Neptune with the standard photochemical model over-predicting the observed CH_3 column abundance. The problem here was less severe than on Saturn, the over-prediction being only 50%. This was with the *Slagle et al.* [1988] expression for k_0 but with k_∞ from *Hessler* [1997]. Note this is the same k_0 and a similar k_∞ that caused the over prediction of a factor of 6 on Saturn. A modest factor of two reduction in K_h from 1×10^7 cm^2 sec^{-1} to 5×10^6 cm^2 sec^{-1} brought the photochemical model in accord with the observations. They found that if they used k_0 from *Macpherson et al.* [1983], the photochemical model then under-predicted the observed methyl column abundance with $K_h = 1 \times 10^7$ cm^2 sec^{-1}. However, as on Saturn, K_h derived from model-observation comparison of the CH_3 emission is lower than that derived from other observations, in this case Voyager UVS observations of CH_4. *Bishop et al.* [1992] derived $K \approx 1-2 \times 10^7$ cm^2 sec^{-1} at the 0.2 μbar level. In comparison for $K_h = 5 \times 10^6$ cm^2 sec^{-1} and $K \propto M^{-1/2}$, $K = 3.3 \times 10^6$ cm^2 sec^{-1} at the 0.2 μbar level, or a factor of 3–6 lower. *Yelle et al.* [1993] derived $K \approx 2-3 \times 10^6$ cm^2 sec^{-1} at the 0.6 μbar level. In comparison for $K_h = 5 \times 10^6$ cm^2 sec^{-1} and $K \propto M^{-1/2}$, $K = 1.7 \times 10^6$ cm^2 sec^{-1} at the 0.6 μbar level, marginally lower and perhaps consistent with the UVS data. But note this is with the slow k_0 of *Slagle et al.* [1988] and thus the use of k_0 that solves the CH_3 over production problem for Saturn would cause a CH_3 under production for Neptune.

[52] In Figure 11 we compare k calculated by using the parameters given by *Bézard et al.* [1999], k_0 from *Slagle et al.* [1988] corrected for He and k_∞ from *Hessler* [1997], to the laboratory data. While this equation for k fits the data better than that of *Bézard et al.* [1998], it is still far from perfect. Notably k_0 is still too large at T = 202K and 298K with the effect that the reaction is predicted to remain in the

high-pressure regime at lower pressures than is supported by the data.

[53] *Lee et al.* [2000] proposed a "modified Slagle" expression for k, namely k_∞ from *Baulch et al.* [1992], k_0 from *Slagle et al.* [1988] for T > 300 K, and for T < 300 K

$$k_0 = 1.8 \times 10^{-6} T^{-3.75} e^{\left(-300/T\right)} \tag{22}$$

They also used the Troe [*Troe*, 1977a, 1977b, 1979; *Gilbert et al.*, 1983] extension to the Lindemann expression. Instead of using a $J_{5/2}$ term an F correction factor term is introduced:

$$k = \frac{k_0 k_\infty M}{k_0 M + k_\infty} \times F \tag{23}$$

$$\log(F) = \frac{\log(F_{cent})}{1 + \left[\frac{\log(M/M_c)}{n}\right]^2},$$

$$M_c = \frac{k_\infty}{k_o} \qquad n = 0.75 - 1.27 \times \log(F_{cent}).$$

Lee et al. [2000] used the same F_{cent} as used by *Slagle et al.* [1988] and *Baulch et al.* [1992]:

$$F_{cent} = 0.38 \times e^{-T/73} + 0.62 \times e^{-T/1180} \tag{24}$$

With this expression for the methyl recombination rate, $K_h \approx 1\text{–}2 \times 10^7$ cm^2 sec^{-1} for Saturn and $K_h = 5 \times 10^7$ cm^2 sec^{-1} for Neptune they were able to reproduce the CH_3 observations. (N.B. The altitude profile for K used by *Lee et al.* [2000] is quite different between the two planets; see discussion below.) In addition they made predictions for the abundance of CH_3 on Uranus, Jupiter, and Titan.

[54] In Figure 12 we compare k calculated by using k_0 and k_∞ from *Lee et al.* [2000] to the new laboratory data. Since the data is all for T < 300 K only the low temperature expression for k_0 is of relevance here. While this expression for k fits the laboratory data better than the previous two expressions, it still has its deficiencies. It is too small at T = 155 K and too large at T = 298 K. It is also important to note that in the temperature and pressure range of Figure 12 the pressure dependence of this expression is coming almost completely from the F term. If k_0 and k_∞ were just substituted into the simple Lindemann expression (i.e., equation (8) instead of equation (12)), then k would be predicted to be nearly constant and approximately equal to k_∞.

[55] In summary while much has been made of the temperature dependence of k_0 below room temperature, what is more important is the magnitude of k_0 relative to k_∞. For example, note that the expressions used by *Bézard et al.* [1998] and *Bézard et al.* [1999], based on high temperature data, fit the T = 155 K data better than the T = 298 K data and fit the T = 155 K data better than that of *Lee et al.* [2000], who purposefully modified k_0 to be applicable to low temperature data. In general the modelers have used a value of k_0 relative to k_∞ that is too large. This has the effect of predicting that the reaction remains in the high-pressure limit at lower pressures than is supported by the laboratory data. Since the high-pressure limit is the upper limit to the reaction rate, this results in a faster CH_3 reaction sink and thus a lower predicted CH_3 column abundance. The consequences are non-trivial, as the "standard" photochemical models predict an excess CH_3 column density. And as it is a model-observation comparison that is used to derive constraints on the strength of vertical mixing in the upper atmospheres, inaccuracies in the rate constant imply the same in the derived rate of vertical mixing. While none of the previously used expressions for the methyl recombination rate reproduces the laboratory data better than the expressions obtained here, it has yet to be shown what impact, if any, these new expressions have on the photochemical models.

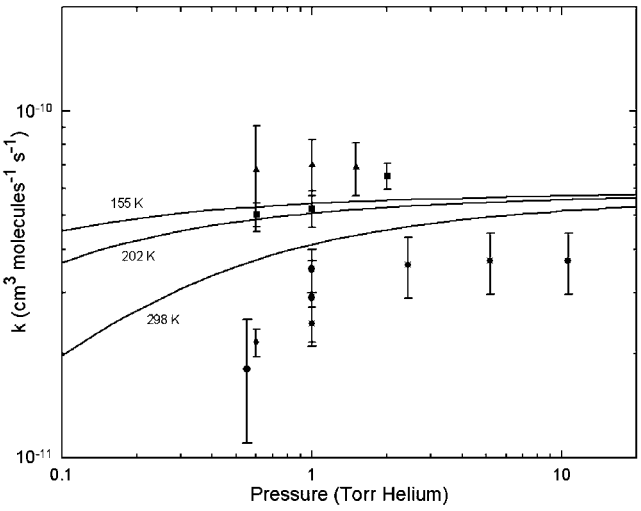

Figure 12. Same as Figure 4 except the curves were generated using the parameters and formula given by *Lee et al.* [2000], with k_0 corrected for He, to model CH_3 profiles for Neptune, Saturn, and Jupiter.

4.2. Model Description

[56] Photochemical calculations were carried out with a one-dimensional hydrocarbon photochemical model. The model takes into account the photolysis and chemical reactions that interlink the hydrocarbons with each other and atomic hydrogen. It solves their coupled continuity equations assuming steady state conditions. The continuity equation for ith species is

$$\frac{-d\Phi_i}{dz_i} + P_i - L_i = 0 \tag{25}$$

where i is an index that runs over species, Φ_i is the flux of the species in molecules cm^{-2} sec^{-1}, z is the altitude, and P_i and L_i are respectively the chemical production and chemical loss rate of the species in molecules cm^{-3} sec^{-1}. The expression for the flux includes terms for both transport (eddy mixing) and molecular diffusion. The model has been most recently described by *Bishop et al.* [1998]. Chemical reactions and kinetic rates included in the modeling are listed in Table 3 of their paper except for the $CH_3 + CH_3$ rate constant where we used the rate expressions as given in

Table 6 and equation (15) of this paper. One-dimensional photochemical models implicitly assume that the atmosphere is horizontally homogeneous. Since the Infrared Space Observatory (ISO) observations are global average observations this means that the model parameters such as length of illuminated day, solar zenith angle, etc. should be representative of midlatitude average values for the model results to be consistent with the observations. If the ISO observations are dominated by small anomalous regions (e.g., hot spots) then there will be an inconsistency between model input parameters and the observations. Photolysis rates were calculated for disk-averaged conditions, and account for both solar irradiance and the Lyman-α skyglow from the local interstellar medium. Solar minimum conditions (Lyman-α flux at 1 AU = 2.69×10^{11} photons cm^{-2} s^{-1}) representative of the time of the ISO observations, were used because the chemical lifetime of CH_3 was found to be shorter than the solar cycle. Larger solar fluxes, average or solar maximum, will result in larger model predicted CH_3 column densities.

4.3. Model Results

4.3.1. Saturn

[57] The derived CH_3 column abundance for P $\leq$ 10 mbar on Saturn from ISO observations is $(6-2.5) \times 10^{13}$ cm^{-2} [*Moses et al.*, 2000]. For the temperature and pressures relevant to Saturn's stratosphere, the Case i expression produces the lowest predicted CH_3 column abundance and Case ii the second lowest. Using the Case i rate constant and $K_h = 10^7$ cm^2 sec^{-1} the model predicted CH_3 column abundance is 5.8×10^{13} cm^{-2}, just within the ISO upper limit. This is also slightly higher than the column abundance predicted by *Lee et al.* [2000], 5.1×10^{13} cm^{-2}, with their "modified Slagle" expression for the rate constant and a slightly higher value of K_h. If we used the "modified Slagle" expression and $K_h = 10^7$ cm^2 sec^{-1} and our altitude profile for K in the photochemical model, the predicted CH_3 column abundance is 6.4×10^{13} cm^{-2}. This is closer to, but still not within, the ISO upper limit, and closer to, but not the same as, the *Lee et al.* [2000] results. The differences between our results and those of *Lee et al.* [2000] probably result from differences in the model atmosphere, K profile, and other CH_3 controlling chemistry. If K_h is reduced to 5×10^6 cm^2 sec^{-1}, then the model predicted CH_3 column abundance is within the ISO derived range for the Case i, ii, and iii rate constant expressions (4.7×10^{13} cm^{-2}, 5.5×10^{13} cm^{-2}, and 5.9×10^{13} cm^{-2} respectively). If we further reduce K_h to 2×10^6 cm^2 sec^{-1} then the model predicted CH_3 column abundance is within the ISO range irrespective of the expression used for the $CH_3 + CH_3$ rate constant (range in predicted CH_3 column densities is $3.7-5.4 \times 10^{13}$ cm^{-2}). Thus the new laboratory data has provided some improvement (compare $K_h = 7 \times 10^5$ cm^2 sec^{-1} if k_0 from *Slagle et al.* [1988] is used to $K_h = 10^7$ cm^2 sec^{-1} if the Case i rate expression is used) but it has not eliminated the problem of CH_3 over-abundance in the models when K_h is derived from CH_4 observations ($K_h \geq 3 \times 10^7$ cm^2 sec^{-1}). The impact of this difference in K_h values on the CH_4 mixing ratio profile can be seen as follows. *Festou and Atreya* [1982] determined that the value of the CH_4 mole fraction was $2.3-1.3 \times 10^{-4}$ where the H_2 number density is 1.2×10^{12} molecules cm^{-3}. At the same atmospheric level, *Smith et al.* [1983] derive a slightly lower value of the CH_4 mole fraction, 6.0×10^{-5}. With $K_h = 10^7$ cm^2 sec^{-1} our photochemical model predicts at this level a CH_4 mole fraction of 4.4×10^{-7}, a value outside the quoted uncertainties of *Festou and Atreya* [1982] and *Smith et al.* [1983].

4.3.2. Neptune

[58] From analysis of ISO observations, *Bézard et al.* [1999] report a nominal CH_3 column abundance for P $\leq$ 0.2 mbar of 1.6×10^{13} molecules cm^{-2} with an allowed range of $(2.8-0.7) \times 10^{13}$ molecules cm^{-2}. For the temperature and pressures relevant to Neptune's stratosphere, the Case i expression produces the lowest predicted CH_3 column abundance; Case ii is the second lowest, as was the case for Saturn. Using the Case i rate constant and $K_h = 10^7$ cm^2 sec^{-1}, the model predicted CH_3 column abundance is 3.7×10^{13} cm^{-2} which is above the ISO upper limit. Reducing K_h to 5×10^6 cm^2 sec^{-1} the model predicted CH_3 column abundance decreases to 2.9×10^{13} cm^{-2}, at or near the ISO upper limit. If K_h is reduced further to 2×10^6 cm^2 sec^{-1} then the model predicted CH_3 column abundance is within the ISO range irrespective of the expression used for the $CH_3 + CH_3$ rate constant (range in predicted CH_3 column densities is $2.0-2.7 \times 10^{13}$ cm^{-2}). This is all for $K \propto M^{-1/2}$ altitude profiles. If instead we use the Case B eddy profile from *Bézard et al.* [1999] with the parameters given above, the result is the same, the model predicted CH_3 column abundance is within the ISO range irrespective of the expression used for the $CH_3 + CH_3$ rate constant (range in predicted CH_3 column densities is $1.8-2.6 \times 10^{13}$ cm^{-2}). The value reported by *Lee et al.* [2000] with their "modified Slagle" expression, 2.2×10^{13} cm^{-2}, lies within this range. Note, however, that the K profile used by *Lee et al.* [2000] has K increasing with decreasing pressure for pressures lower than 10^{-4} mbar (their Figure 2), while the Case B eddy profile from *Bézard et al.* [1999] has K decreasing with decreasing pressure in this same regime. For Neptune, the laboratory data have given no relief from the problem of CH_3 over-abundance in the models when K_h is derived from CH_4 observations, though as before the problem is less severe on Neptune than on Saturn.

5. Summary and Conclusions

[59] Using the CH_3 recombination rates derived here and the ISO CH_3 observations, we derive for Saturn $K_h \leq 1 \times 10^7$ cm^2 sec^{-1} while higher values are found when K_h is derived from CH_4 and other observations, $K_h \geq 3 \times 10^7$ cm^2 sec^{-1}. For Neptune we find for $K \propto M^{-1/2}$ $K_h \leq 5 \times 10^6$ cm^2 sec^{-1}. For this type of profile K_h is either a factor of 3–6 lower or consistent with the Voyager UVS CH_4 observations (*Bishop et al.* [1992] versus *Yelle et al.* [1993]). Alternatively, if K follows a Case B eddy profile from *Bézard et al.* [1999] with the parameters given in section 4, the ISO CH_3 observations are reproduced. But it is not possible to say that the Case B profile matches the UVS data as the parameters are sufficiently different from the profile of this type used by *Romani et al.* [1993] to reproduce the UVS observations. Note that to minimize the difference between K_h derived from modeling the CH_3 emission with K_h from other observations requires using the fastest possible rate expression for $CH_3 + CH_3$ consis-

tent with the data and pushing the ISO derived CH_3 column abundance to its upper limit. In principle, the value of K_h derived from the methane data should be more reliable than that from the CH_3 data as the methane mixing ratio profile is predominately controlled by mixing, unlike that of CH_3 which is controlled by a combination of mixing and chemistry. While the low temperature $CH_3 + CH_3$ laboratory data and the derived recombination rates presented here have reduced the disparity in the derived K_h's for Saturn, they have not done so for Neptune.

[60] One possible reason for differences in the derived K_h for Neptune is temporal variability of K_h as has been suggested for Jupiter [*Atreya et al.*, 1982]. The ISO observations occurred in 1997 while the Voyager encounter with Neptune occurred in 1989. For Saturn this is a more problematical explanation as the derived value of K_h by *Drossart et al.* [1999], based on ISO observations of CH_4 fluorescence, is contemporaneous with the ISO CH_3 observations and consistent with the Voyager derived values of K_h.

[61] On the basis of this study, the solution to the remaining excess CH_3 prediction in the models relative to the ISO data likely lies, to a large extent, elsewhere in the CH_3 photochemistry or transport, not in the $CH_3 + CH_3$ rate. If the problem is an underestimation of a sink for CH_3, the possibilities include a missing reaction, a rate constant that is too low (most likely due to extrapolation into the low temperature, low pressure regime), or too small of a cross section of CH_3 photolysis and uncertainty concerning the photolysis products. For the case of a missing reaction it is most likely a two-body reaction considering the pressure regime where CH_3 production and loss occurs. The combination reaction of CH_3 with thermal H has been discussed previously by, e.g., *Moses et al.* [2000] and *Atreya et al.* [1999]. An example of a missing reaction may be the two-body abstraction reaction of CH_3 with hot H atoms as suggested by *Atreya et al.* [1999]. The rate constant for the reaction $CH_3 + H \rightarrow CH_2 + H_2$ is

$$k = 1.0 \times 10^{-10} e^{-7600/T} \tag{26}$$

which yields an activation energy of 63 kJ $mole^{-1}$ [*Baulch et al.*, 1992]. While this amount of energy is not available thermally for the H atoms, it is possible for H atoms produced via Lyman-α photolysis of CH_4 to $CH_3 + H$. This mechanism does provide a plausible reason for the smaller disparity on Neptune in comparison to Saturn as this mechanism is driven by the solar flux. However, determining the fraction of the available excess energy that ends up in the H atom fragment and the competition between thermalization of the H atoms versus breaking apart CH_3 molecules is beyond the scope of this paper. In a similar vein, an argument can be made for a reexamination of CH_3 photolysis in the models on the basis that the problem is worse on Saturn (higher solar UV flux) than on Neptune. For this mechanism to work the products of major CH_3 photolysis would have to be different from what is currently used:

$$CH_3 + h\nu \rightarrow {}^1CH_2 + H \tag{27}$$

This is because $^1CH_2$ is efficiently recycled back to CH_3 via:

$$^1CH_2 + H_2 \rightarrow CH_3 + H \tag{18}$$

[62] Increasing the overall CH_3 photolysis rate in the model for Saturn with $K_h = 2 \times 10^7 cm^2\ sec^{-1}$ in ad hoc manner by a factor of 10 had only a 10% reduction in the model predicted CH_3 column. It is also possible than the problem lies on the other side of the CH_3 photochemical equation with a predicted source being too strong. A possible candidate here is the reaction $H + C_2H_5 \rightarrow 2\ CH_3$ for which there are limited laboratory studies, especially below room temperature. It is of course possible that the solution lies in some combination of the two, e.g., sinks and sources. For completeness sake there is also the "modeler's friend", i.e., the problem lies with the interpretation and analysis of the CH_3 emission data. The exact reconciliation of this problem is outside the scope of this paper.

[63] Given this problem, it is then important to keep in mind the natural tendency to use rate constants that allow the model to best match the data. In this case that would be to use the fastest CH_3 recombination rate expression, either Case i or ii. However, this may only serve to mask the problem of the over prediction of CH_3 and make it harder to uncover the real solution to the problem. On the basis of the laboratory data we can not exclude the slowest rate expressions, Cases iv and the J formalism.

[64] **Acknowledgments.** This work was supported by the NASA Planetary Atmospheres Research Program. We thank Walter Payne (GSFC) for assistance in the early stages of this study. We thank Zhuangjie Li (Univ. of Illinois) for sharing with us his design for the glass-to-metal coupling of the jacketed Pyrex flow tube to the stainless-steel mass spectrometer chamber. Floyd Hunsaker (GSFC) and Mike Trembly (Glass Tech) contributed significantly to the adaptation of this design to our system.

References

Atreya, S. K., Eddy mixing coefficient on Saturn, *Planet. Space Sci.*, *30*, 849–854, 1982.

Atreya, S. K., M. C. Festou, T. M. Donahue, R. B. Kerr, E. S. Barker, W. D. Cochran, J. L. Bertaux, and W. L. Upson II, Copernicus measurements of the Jovian Lyman-alpha emission and its aeronomical significance, *Astrophys. J.*, *262*, 377–387, 1982.

Atreya, S. K., S. G. Edington, T. Encrenaz, and H. Feuchtgruber, ISO observations of C_2H_2 on Uranus and CH_3 on Saturn: Implications for atmospheric vertical mixing in the Voyager and ISO epochs, and a call for relevant laboratory measurements, in *The Universe as Seen by ISO, Eur. Space Agency Spec. Publ., ESA SP-427*, 149–152, 1999.

Baulch, D. L., et al., Evaluated kinetic data for combustion modelling, *J. Phys. Chem. Ref. Data*, *21*(3), 411–734, 1992.

Bezard, B., H. Feuchtgruber, J. I. Moses, and T. Encrenaz, Detection of methyl radicals (CH_3) on Saturn, *Astron. Astrophys.*, *334*, L41–L43, 1998.

Bezard, B., P. N. Romani, H. Feuchtgruber, and T. Encrenaz, Detection of methyl radicals on Neptune, *Astrophys. J.*, *515*, 868–872, 1999.

Bishop, J., S. K. Atreya, P. N. Romani, B. R. Sandel, and F. Herbert, Voyager 2 ultraviolet spectrometer solar occultations at Neptune: Constraints on the abundance of methane in the stratosphere, *J. Geophys. Res.*, *97*, 11,681–11,694, 1992.

Bishop, J., S. K. Atreya, P. N. Romani, G. S. Orton, B. R. Sandel, and R. V. Yelle, The middle and upper atmosphere of Neptune, in *Neptune and Triton*, edited by D. P. Cruikshank, pp. 427–487, Univ. of Ariz. Press, Tucson, 1995.

Bishop, J., P. N. Romani, and S. K. Atreya, Voyager 2 ultraviolet spectrometer solar occultations at Neptune: Photochemical modeling of the 125–165 nm lightcurves, *Planet. Space Sci.*, *46*, 1–20, 1998.

Brunning, J., and L. J. Stief, Kinetic studies of the reaction of the SO radical with NO_2 and ClO from 210 to 363 K, *J. Chem. Phys.*, *84*, 4371–4377, 1986.

Clyne, M. A. A., and A. J. MacRobert, Kinetic studies of free radical reactions by mass spectrometry. I. The reactions SO + NO_2 and ClO + NO, *Int. J. Chem. Kinet.*, *12*, 79–96, 1980.

Clyne, M. A. A., and R. T. Watson, Kinetic studies of diatomic free-radicals using mass spectrometry. 1. System description and applications to F atoms and FO radicals, *J. Chem. Soc. Faraday Trans. 1*, *70*, 1109–1123, 1974.

Cody, R. J., W. A. Payne, R. P. Thorn, F. L. Nesbitt, M. A. Iannone, D. C. Tardy, and L. J. Stief, Rate constant for the recombination reaction $CH_3 + CH_3 \rightarrow C_2H_6$ at T = 298 and 202 K, *J. Phys. Chem. A*, *106*, 6060–6067, 2002.

DeMore, W. B., S. P. Sander, D. M. Golden, R. F. Hampson, M. J. Kurylo, C. J. Howard, A. R. Ravishankara, C. E. Kolb, and M. J. Molina, Chemical kinetics and photochemical data for use in stratospheric modeling: Evaluation number 12, *JPL Publ.*, *97-4*, 1–266, 1997.

Deters, R., M. Otting, H. G. Wagner, F. Temps, B. Laszlo, S. Dobe, and T. Berces, A direct investigation of the reaction CH_3 + OH: Overall rate constant and CH_2 formation at T = 298 K, *Ber. Bunsen. Ges. Phys. Chem.*, *102*, 58–72, 1998a.

Deters, R., M. Otting, H. G. Wagner, F. Temps, and S. Dobe, Rate constant for the reaction $CH_3 + CH_2(X)$ at 298 K, *Ber. Bunsen. Ges. Phys. Chem.*, *102*, 978–981, 1998b.

Drossart, P., T. Fouchet, J. Crovisier, E. Lellouch, T. Encrenaz, H. Feuchtgruber, and J.-P. Champion, Fluorescence in the 3 micron bands of methane on Jupiter and Saturn from ISO/SWS observations, in *The Universe as Seen by ISO, Eur. Space Agency Spec. Publ., ESA SP-427*, 169–172, 1999.

Festou, M. C., and S. K. Atreya, Voyager ultraviolet stellar occultation measurements of the composition and thermal profiles of the Saturnian upper atmosphere, *Geophys. Res. Lett.*, *9*, 1147–1150, 1982.

Forst, W., *Theory of Unimolecular Reactions*, Academic, San Diego, Calif., 1973.

Gilbert, R. G., K. Luther, and J. Troe, Theory of thermal unimolecular reactions in the fall-off range. II. Weak collision rate constants, *Ber. Bunsen. Ges. Phys. Chem.*, *87*, 169–177, 1983.

Hessler, J. P., The use of Monte Carlo simulations to evaluate kinetic data and analytic approximations, *Int. J. Chem. Kinet.*, *29*, 803–817, 1997.

Hessler, J. P., and P. J. Ogren, Recombination of methyl radicals. 2. Global fits of the rate coefficient, *J. Phys. Chem. A*, *100*, 984–992, 1996.

Hinshelwood, C. N., *The Kinetics of Chemical Change*, Oxford at the Clarendon Press, London, 1940.

Holbrook, K. A., M. J. Pilling, and S. H. Robertson, *Unimolecular Reactions*, 2nd ed., John Wiley, Hoboken, N. J., 1996.

Hunten, D. M., Vertical transport in atmospheres, in *Atmospheres of Earth and the Planets*, edited by B. M. McCormac, pp. 59–72, D. Reidel, Norwell, Mass., 1975.

Klippenstein, S. J., and L. B. Harding, A direct transition state theory based study of methyl radical recombination kinetics, *J. Phys. Chem. A*, *103*, 9388–9398, 1999.

Lee, A. Y. T., Y. L. Yung, and J. Moses, Photochemical modeling of CH_3 abundances in the outer solar system, *J. Geophys. Res.*, *105*, 20,207–20,225, 2000.

Lindemann, F. A., Discussion on radiation theory of chemical action, *Trans. Faraday Soc.*, *17*, 598–599, 1922.

Macpherson, M. T., M. J. Pilling, and J. C. Smith, The pressure and temperature dependence of the rate constant for methyl radical recombination over the temperature range 296–577 K, *Chem. Phys. Lett.*, *94*, 430–433, 1983.

Marcus, R. A., Unimolecular dissociations and free-radical recombination reactions, *J. Chem. Phys.*, *20*, 359–364, 1952.

Marcus, R. A., and O. K. Rice, Session on free radicals: The kinetics of the recombination of methyl radicals and iodine atoms, *J. Phys. Colloid Chem.*, *55*, 894–908, 1951.

Marrero, T. R., and E. A. Mason, Gaseous diffusion coefficients, *J. Phys. Chem. Ref. Data*, *1*, 3–118, 1972.

Moses, J. I., B. Bezard, E. Lellouch, G. R. Gladstone, H. Feuchtgruber, and M. Allen, Photochemistry of Saturn's atmosphere. I. Hydrocarbon chemistry and comparisons with ISO observations, *Icarus*, *143*, 244–298, 2000.

Oref, I., General expression for unimolecular rate coefficients in the falloff region, *J. Phys. Chem.*, *93*, 3465–3469, 1989.

Oref, I., and D. C. Tardy, Energy transfer in highly excited large polyatomic molecules, *Chem. Rev.*, *90*(8), 1407–1445, 1990.

Parkes, D. A., D. M. Paul, and C. P. Quinn, Study of the spectra and recombination kinetics of alkyl radicals by molecular modulation spectrometry, *J. Chem. Soc. Faraday Trans. 1*, *72*, 1935–1951, 1976.

Parkinson, C. D., E. Griffioen, J. C. McConnell, G. R. Gladstone, and B. R. Sandel, He 584 Å dayglow on Saturn: A reassessment, *Icarus*, *133*, 210–220, 1999.

Pawlowska, Z., and I. Oref, A general expression for weak collision unimolecular rate coefficients in the falloff region, *J. Phys. Chem.*, *94*, 567–576, 1990.

Robertson, S. H., M. J. Pilling, D. L. Baulch, and N. J. B. Green, Fitting of pressure-dependent kinetic rate data by master equation/inverse Laplace transform analysis, *J. Phys. Chem.*, *99*, 13,452–13,460, 1995.

Romani, P. N., J. Bishop, B. Bezard, and S. Atreya, Methane photochemistry on Neptune: Ethane and acetylene mixing ratios and haze production, *Icarus*, *106*, 442–463, 1993.

Sandel, B. R., J. C. McConnell, and D. F. Strobel, Eddy diffusion at Saturn's homopause, *Geophys. Res. Lett.*, *9*, 1077–1080, 1982.

Slagle, I. R., D. Gutman, J. W. Davies, and M. J. Pilling, Study of the recombination reaction $CH_3 + CH_3 \rightarrow C_2H_6$: 1. Experiment, *J. Phys. Chem.*, *92*, 2455–2462, 1988.

Smith, G. R., D. E. Shemansky, J. B. Holberg, A. L. Broadfoot, B. R. Sandel, and J. C. McConnell, Saturn's upper atmosphere from the Voyager 2 EUV solar and stellar occultations, *J. Geophys. Res.*, *88*, 8667–8678, 1983.

Smith, S. C., and R. G. Gilbert, *Theory of Unimolecular and Recombination Reactions*, Blackwell Sci., Malden, Mass., 1990.

So, H. Y., and R. C. Dunbar, Photodissociation of gas-phase halogenated benzene radical cations, *J. Chem. Phys.*, *90*, 2192–2200, 1989.

Stoliarov, S. I., V. D. Knyazev, and I. R. Slagle, Experimental study of the reaction between vinyl and methyl radicals in the gas phase: Temperature and pressure dependence of overall rate constants and product yields, *J. Phys. Chem. A*, *104*, 9687–9697, 2000.

Tardy, D. C., and B. S. Rabinovitch, Intermolecular vibrational energy transfer in thermal unimolecular systems, *Chem. Rev.*, *77*(3), 369–408, 1977.

Troe, J., Theory of thermal unimolecular reactions at low pressures. I. Solutions of the master equation, *J. Chem. Phys*, *66*, 4745–4757, 1977a.

Troe, J., Theory of thermal unimolecular reactions at low pressures. II. Strong collision rate constants: Applications, *J. Chem. Phys.*, *66*, 4758–4775, 1977b.

Troe, J., Predictive possibilities of unimolecular rate theory, *J. Phys. Chem.*, *83*, 114–126, 1979.

Walter, D., H. H. Grotheer, J. W. Davies, M. J. Pilling, and A. F. Wagner, Experimental and theoretical study of the recombination reaction $CH_3 + CH_3 \rightarrow C_2H_6$, *Symp. Int. Combust. Proc.*, *23*, 107–113, 1990.

Yelle, R. V., F. Herbert, B. R. Sandel, R. J. Vervack Jr., and T. M. Wentzel, The distribution of hydrocarbons in Neptune's upper atmosphere, *Icarus*, *104*, 38–59, 1993.

R. J. Cody, P. N. Romani, and L. J. Stief, Laboratory for Extraterrestrial Physics, NASA Goddard Space Flight Center, Code 691, Greenbelt, MD 20771, USA. (regina.cody@nasa.gov)

M. A. Iannone, Department of Chemistry, Millersville University, Millersville, PA 17551, USA.

F. L. Nesbitt, Department of Chemistry, Catholic University of America, Washington, DC 20064, USA.

D. C. Tardy, Department of Chemistry, University of Iowa, Iowa City, IA 52242, USA.